

Article

Thermodynamics and Magnetism of YCo_5 Compound Doped with Fe and Ni: An Ab Initio Study

Alexander Landa * , Per Söderlind, Emily E. Moore  and Aurelien Perron

Lawrence Livermore National Laboratory, Livermore, CA 94551-0808, USA; soderlind@llnl.gov (P.S.); moore255@llnl.gov (E.E.M.); perron1@llnl.gov (A.P.)

* Correspondence: landa1@llnl.gov

Received: 3 August 2020; Accepted: 28 August 2020; Published: 31 August 2020



Abstract: YCo_5 permanent magnet exhibits high uniaxial magnetocrystalline anisotropy energy and has a high Curie temperature. These are good properties for a permanent magnet, but YCo_5 has a low energy product, which is notably insufficient for a permanent magnet. In order to improve the energy product in YCo_5 , we suggest replacing cobalt with iron, which has a much bigger magnetic moment. With a combination of density-functional-theory calculations and thermodynamic CALculation of PHase Diagrams (CALPHAD) modeling, we show that a new magnet, $\text{YFe}_3(\text{Ni}_{1-x}\text{Co}_x)_2$, is thermodynamically stable and exhibits an improved energy product without significant detrimental effects on the magnetocrystalline anisotropy energy or the Curie temperature.

Keywords: density-functional theory; thermodynamic modeling; rare earths; permanent magnets; anisotropy; curie temperature; enthalpy

1. Introduction

Three principal material parameters define the intrinsic properties of hard magnetic materials: (i) spontaneous (saturation) magnetization, M_s , (ii) Curie temperature, T_c , and (iii) magnetocrystalline anisotropy energy (MAE), characterized by its first-order anisotropy coefficient, K_1 [1]. These three parameters all need to be large for an economically effective permanent magnet, i.e., $T_c \sim \geq 550$ K, $M_s \sim \geq 1$ MA/m, $K_1 \sim \geq 4$ MJ/m³. By incorporating transition-metal (TM) with rare-earth-metal (RE) atoms in numerous intermetallic compounds [1,2], one produces a material with these fascinating magnetic properties.

In our previous papers [3,4], we suggested a new economically effective permanent magnet, SmFe_3CoNi , that was developed from the well-known SmCo_5 blueprint. More contemporary neodymium magnets of the Nd-Fe-B type are superior to the SmCo_5 magnet because of their greater maximum energy product emerging from their iron-rich stoichiometry. Our proposed SmFe_3CoNi magnet, however, eliminated most of the detriment of the SmCo_5 magnet while maintaining its superior high-temperature effectiveness over neodymium magnets.

According to ref. [5], the price of Sm and Co is moderately high, which makes reducing the price of the SmCo_5 magnet a dominant objective. The authors [5] claim that the rare-earth (RE) Y (225 RMB/kg) is cheaper than Sm (450 RMB/kg), and by limited substitution of Sm with Y atoms, a high performance ($\text{Sm}_{1-x}\text{Y}_x$) Co_5 magnet can be prepared. The YCo_5 compound (the CaCu_5 -type structure) is isostructural with SmCo_5 . The YCo_5 magnet exhibits significant MAE of $K_1 \sim 6.5$ MJ/m³ (3.41 meV/f.u.) [6], which is excessive compared to that of the $\text{Nd}_2\text{Fe}_{14}\text{B}$ (Neomax) magnets ($K_1 \sim 4.9$ MJ/m³, [7]). It furthermore has a Curie temperature ($T_c \sim 987$ K, [6]) almost twice that of the Neomax ($T_c \sim 588$ K, [7]). However, $\text{Nd}_2\text{Fe}_{14}\text{B}$ presently prevails the worlds wholesale for permanent magnets ($\sim 62\%$) [8,9] because it has the biggest energy production sustained by its record energy product ($(BH)_{max} \sim 512$ kJ/m³ [7], more than twice that of the YCo_5 magnets, $(BH)_{max} = 224$ kJ/m³ [10,11].

The YCo₅ magnet is probably the most studied magnet with the CaCu₅-type structure. It has been explored both experimentally and theoretically in the past due to its unique qualification as a “gap” permanent magnetic material [5,10–84]. Actually, almost all experimental papers on the YCo₅ magnet have been dedicated to studying MAE of the undoped magnet as well as doped with Sm, Nd, Ge, Fe, Cu, and Ni [5,10–20,22–29,31–35,41–43,52–54,62,66,70,72–74,77,80]. MAE, the Curie temperature, and the energy product, which are 5.7 MJ/m³, 921 K, and 224 kJ/m³, correspondingly, were first reported in refs. [10–12]. Slightly higher values, $K_1 \sim 6.4$ MJ/m³ and $T_c \sim 987$ K, were reported in ref. [15]. According to Schweitzer and Tasset [28], the Curie temperature is $T_c \sim 920$ K. Ermolenko [17] studied the temperature dependence of MAE of the YCo₅ magnet. Later, similar measurements were performed by Al-Omari et al. [54]. Refs. [20,22] represent the first review papers dedicated to the experimental study of the YCo₅ magnet, although Buschow [20] claimed that the total magnetic moment of YCo₅ is equal to $m^{(tot)} = 7.52 \mu_B/f.u.$ Higher values of the total magnetic moment for YCo₅, $m^{(tot)} = 8.33 \mu_B/f.u.$, and MAE, $K_1 \sim 7.38$ MJ/m³, were also reported [29].

In regard to the SmCo₅ magnet, the MAE is dominated by the 3D electron contribution from Co, although the localized Sm 4f electrons are believed to influence MAE somewhat [3]. For YCo₅, on the other hand, magnetic anisotropy is entirely due to the Co 3d electrons because Y has no electrons occupying 4f states [16,18,19,23–25,28]. According to Refs. [16,18,23,25,28,70], the spin-polarized neutron scattering, inelastic spin flip-neutron scattering, nuclear magnetic resonance (NMR), neutron diffraction (ND), and x-ray magnetic circular dichroism (XMCD) measurements of YCo₅ revealed a very large orbital contribution to the total magnetic moment from Co₁(2c) sites, indicating that the large axial MAE of the YCo₅ magnet arises from the Co₁(2c) sites. The orbital moment on the Co₂(3g) sites is smaller than the orbital moment on the Co₁(2c) sites and contributes to the planar MAE of the YCo₅ magnet [23,25].

Several experimental studies of doping the RECo₅ compound with Fe or Ni [14,31] suggest that iron atoms prefer to occupy 3g sites because they are slightly larger than cobalt atoms and are more easily accommodated in these positions. On the other hand, there are vigorous manifestations that nickel atoms conversely occupy 2c sites. According to ref. [31], the compositional dependency of the lattice constant and the interatomic distances can be satisfactorily justified by nickel atoms occupying 2c rather than 3g sites in the RECo₅ compound. Copper atoms choose to occupy 3g sites because the atomic volume of copper is bigger than that of cobalt atoms and even bigger than that of iron atoms [31].

From a price standpoint, it is profitable to replace Co atoms with Fe because of the abundance of Fe in the Earth's crust compared to Co (by a factor of ~ 2000) making a Fe-containing magnet economically more attractive. Furthermore, Fe is a ferromagnetic metal with a very substantial magnetization at room temperature (1.76 MA/m [7]). The YCo₅ magnet doped with iron has been the subject of numerous experimental papers [13,18,20,34,35,41,42,52,72,73,80]. Replacing all cobalt with iron to enhance magnetization in the YFe₅ compound produces a thermodynamically unstable phase, which is not experimentally observed within the equilibrium Y-Fe phase diagram. Contrarily, the Y(Co_{1-x}Fe_x)₅ compounds (CaCu₅-type) have been observed, with x ranging from 0.2 to 0.4 [42,52]. Moreover, the Curie temperature of the Y(Co_{1-x}Fe_x)₅ alloys has been found to increase from ~ 930 K to ~ 1020 K when varying across increasing x from 0.0 to 0.2 [42], contrary to the Y₂(Co_{1-x}Fe_x)₁₇ alloys that display a monotonic reduction in the Curie temperature with rising Fe amount. The orbital moment is also bigger in cobalt compared to iron, and a decrease of the MAE is thus expected for $x > 0$. The lattice constant and magnetization also enhance with x from 0 to 0.4 [52] in the Y(Co_{1-x}Fe_x)₅ alloys.

In addition to iron and nickel, copper has also been used to dope the YCo₅ magnet [20,28,31,33,50,52,53]. In contrast to the Y(Co_{1-x}Fe_x)₅ system, Y(Co_{1-x}Ni_x)₅ and Y(Co_{1-x}Cu_x)₅ compounds are stable across the entire composition domain (i.e., $x = 0-1$). Substituting cobalt atoms with nickel or copper atoms gradually decreases magnetization and magnetic anisotropy. By connecting diffraction techniques and electron microscopy, Colin et al. [66] studied the solubility restriction of Ge

in the $Y(\text{Co}_{1-x}\text{Ge}_x)_5$ alloys. A preferential substitution of Ge atoms that were larger than Co atoms on the 3g positions was observed.

Numerous theoretical approaches have been used to study the YCo_5 magnets. These include augmented-plane-waves (APW), point charge, linearized muffin-tin orbitals within atomic sphere approximation (LMTO-ASA), Haydock recursion (HR), full-potential linearized augmented-plane-waves (FLAPW), linear combination of atomic orbitals (LCAO), pseudopotential projected augmented waves (VASP-PAW), augmented spherical waves (ASW-ASA), full-potential linear muffin-tin orbitals (FPLMTO), dynamical mean field theory in conjunction with density functional theory (LDA-DMFT), and Korringa–Kohn–Rostoker multiple-scattering formulation in conjunction with the coherent potential approximation and disordered local moment approximation (KKRASA-CPA-DLM) [21,26,27,30,37–40,44–51,55–65,67,68,70,71,74–79,81–84]. According to the self-consistent APW calculations [21], the total moment of the YCo_5 magnet is equal to $m^{(tot)} = 7.31 \mu_B/\text{f.u.}$, which is in accordance with the initially reported experimental data, $m^{(tot)} = 7.52 \mu_B/\text{f.u.}$ [20]. Using the point charge model, Inomata [30] confirmed the conclusion presented in the experimental papers [8,16,19,23,25,28], namely, the orbital moments of Co atoms located on the 2c sites contribute to the axial (positive) MAE of YCo_5 , and the orbital moments of Co atoms located on the 3g sites contribute to its planar (negative) contribution. The importance of the orbital polarization (OP) has been emphasized in LMTO-ASA papers [37–40,45–47]. The magnetization of the YCo_5 compound doped by Ni, $Y(\text{Co}_{5-x}\text{Ni}_x)$ has been studied within the Haydock recursion method [44]. According to these calculations, when the amount of Ni dissolved in the YCo_5 magnet reaches 60%, the YCo_2Ni_3 compound loses its magnetization. The LMTO-ASA formalism has also been applied to study the $Y(\text{Co}_{1-x}\text{Ni}_x)_5$ alloys [48,51]. These calculations confirm that the nickel atoms choose to occupy 2c sites. LCAO calculations by Zhang et al. [49] reveal the total magnetic moment of the YCo_5 magnet is equal to $m^{(tot)} = 8.70 \mu_B/\text{f.u.}$ Steinbeck et al. [55,56] performed fully relativistic LCAO calculations of MAE of YCo_5 and $Y(\text{Co}_{1-x}\text{Fe}_x)_5$ compounds. Their calculated MAE of the YCo_5 magnet is $K_1 = 1.11 \text{ MJ/m}^3$ and $K_1 = 8.40 \text{ MJ/m}^3$ for SOC and SOC+OP theory (where SOC means spin-orbit coupling), correspondingly. They furthermore obtained within the SOC+OP scheme the orbital moments that are $0.33 \mu_B$ and $0.26 \mu_B$ for 2c and 3g sites, correspondingly. These moments are in accordance with experimental measurements of $0.26 \mu_B$ (2c) and $0.24 \mu_B$ (3g) [28]. Calculated MAE for the $Y(\text{Co}_{1-x}\text{Fe}_x)_5$ compounds show qualitative agreement with the experimental data [34]. The calculated Curie temperature of the YCo_5 magnet $T_c = 998 \text{ K}$ [57] is in good accord with results of the previous calculations by Wohlfarth [26,27] and the experimental data, $T_c \sim 987 \text{ K}$ [6].

Using FLAPW (without OP), Larson et al. [58–61] calculated MAE of the YCo_5 magnet ($K_1 = 2.83 \text{ MJ/m}^3$) as well as $Y(\text{Co}_{1-x}\text{Fe}_x)_5$ and $Y(\text{Co}_{1-x}\text{Cu}_x)_5$ alloys. Calculated MAE of the $Y(\text{Co}_{1-x}\text{Fe}_x)_5$ compounds is in qualitative accord with the results of the previously mentioned LCAO calculations [56]. MAE of the $Y(\text{Co}_{1-x}\text{Fe}_x)_5$ magnets with 6–7 % doping increases by about 1.9 MJ/m^3 before falling rapidly with a larger Fe doping. The total magnetic moment gradually increases from $m^{(tot)} = 7.2 \mu_B/\text{f.u.}$ (YCo_5) to $\sim 10 \mu_B/\text{f.u.}$ ($Y(\text{Co}_1\text{Fe}_4)$) then falls to $9 \mu_B/\text{f.u.}$ for YFe_5 .

When doping the YCo_5 magnet with copper, the total moment gradually decreases with increasing copper concentration, and finally the moment disappears for the $Y(\text{Co}_1\text{Cu}_4)$ compound. The calculations performed by Larson and Mazin [61] show that, for the $Y(\text{Co}_{1-x}\text{Cu}_x)_5$ alloys, the total magnetic moment decreases linearly with Cu doping, identical to the results of Ni doping of the $Y(\text{Co}_{1-x}\text{Ni}_x)_5$ alloys [51]. However, in contrast to the $Y(\text{Co}_{1-x}\text{Ni}_x)_5$ compounds, the magnetic moments of the cobalt atoms are reasonably local and barely impacted by Cu doping of the $Y(\text{Co}_{1-x}\text{Cu}_x)_5$ alloys until $x \sim 0.5$, where the moment promptly falls to a small value before steadily decreasing [61]. The authors [61] concluded that cobalt in the doped YCo_5 compounds can occur either in a high- or a low-spin state, depending on the local surroundings. A similar conclusion (the high spin to the low spin transition) is presented in the paper of Wu et al. [63], where VASP-PAW formalism is applied to study the $Y(\text{Co}_{1-x}\text{Ag}_x)_5$ alloys.

The ASW-ASA formalism has been applied for study magnetic and electronic properties of the $Y(\text{Co}_{1-x}\text{Fe}_x)_5$ compounds: YCo_5 , $Y(\text{Fe}_2\text{Co}_3)$, $Y(\text{Fe}_3\text{Co}_2)$, and YFe_5 [65]. FPLMTO calculations for the

$Y(\text{Co}_{1-x}\text{Fe}_x)_5$ compounds with $x = 0, 0.1, 0.2,$ and 0.3 [67] confirm that iron atoms choose to occupy 3g sites, and total magnetization increases from $7.50 \mu_B/\text{f.u.}$ to $8.97 \mu_B/\text{f.u.}$ with increasing x from 0 to 0.3 because iron atoms have a much bigger magnetic moment ($\sim 2.4 \mu_B$) than the magnetic moment of cobalt atoms ($\sim 1.5 \mu_B$).

A real-space pseudopotential formalism with SOC incorporated by norm-conserving pseudopotentials has been used to compute MAE of the YCo_5 magnet in different structures [78]. It appears that the authentic CaCu_5 -type structure (Space Group $P6/mmm$) possesses the largest total magnetic moment $m^{(tot)} = 7.13 \mu_B/\text{f.u.}$ and MAE $K_1 = 2.68 \text{ MJ/m}^3$. The latter is, however, significantly smaller than the experimental value of $K_1 = 6.5 \text{ MJ/m}^3$ [6].

Nguyen et al. [79] studied the dependence of MAE of the YCo_5 magnet with intra-atomic Coulomb interaction (the Hubbard U parameter, DFT+ U scheme) and strength of SOC within the PAW-VASP method. These calculations showed that, for GGA+ U calculations, with $1.4 \text{ eV} \leq U \leq 1.47 \text{ eV}$ and $J = 0.8 \text{ eV}$, MAE of the YCo_5 compound changes within the experimentally observed range. Similar results are presented in the work of Zhu et al. [70], where LDA+DMFT computational scheme is used to replace the OP correction [37]. The LDA+DMFT calculations suggest that electron correlation effects play an essential role in the formation and the enhancement of orbital moments and magnetic anisotropy in the YCo_5 magnet. ND, XRD measurements, and FPLMTO-DMFT technique have been used [77] to describe an isomorphic (without change of the symmetry) lattice collapse and the electronically topological transition (ETT), which is the first order Lifshitz phase transition in the YCo_5 magnet at pressure about $18 \pm 2 \text{ GPa}$ first reported in refs. [62,63] based on XRD measurements and FPLO calculations [66]. According to these calculations, the Curie temperature of the YCo_5 magnet, $T_c \approx 987 \text{ K}$, is in the range of experimental measurements. These calculations reveal that, at ambient pressure, the orbital moments are $0.22 \mu_B$ and $0.18 \mu_B$ for 2c and 3g, correspondingly, and at pressure of 7.2 GPa , the orbital moments are $0.18 \mu_B$ and $0.15 \mu_B$ for 2c and 3g, correspondingly, which is in reasonable agreement with the experimental observation [28] (at ambient pressure) and also in agreement with results of LDA-DMFT calculations [70]. The atom-resolved $\text{Co}_1(2c)$ and $\text{Co}_2(3g)$ orbital moments reach the maximum values for the Coulomb parameter $U \sim 2 \text{ eV}$. These results for the orbital moments are consistent with previous XMCD measurements [71], inelastic spin flip-neutron scattering experiments [16], and OP calculations [37,55,56].

The temperature dependence of MAE and the spontaneous magnetization of the YCo_5 magnet has been calculated by utilizing the relativistic KKRASA-CPA-DLM approach [71,74–76,81,82]. The calculated total magnetic moment, $m^{(tot)}$, is $8.50 \mu_B/\text{f.u.}$ $8.03 \mu_B/\text{f.u.}$ at 0 K and around $T = 100 \text{ K}$, correspondingly, [71], which is in a fair accord with the experimental data, $8.33 \mu_B/\text{f.u.}$, at liquid-helium temperature [29], and $7.99 \mu_B/\text{f.u.}$ at room temperature [28]. Calculated MAE is equal to $K_1 \sim 4.63 \text{ MJ/m}^3$ at $T \approx 50 \text{ K}$ [71], which is larger than reported in the previous calculations, $K_1 \sim 2.83 \text{ MJ/m}^3$ at $T = 0 \text{ K}$ [58–61] (see Figure 1, [71]), but smaller than the experimental value of $K_1 \sim 7.38 \text{ MJ/m}^3$ at $T = 4.2 \text{ K}$ [24], $K_1 \sim 6.40 \text{ MJ/m}^3$ at $T = 77 \text{ K}$ [15] as well as $K_1 \sim 6.03 \text{ MJ/m}^3$ [15], $K_1 \sim 5.50 \text{ MJ/m}^3$ [69], and $K_1 \sim 5.00 \text{ MJ/m}^3$ [17] at room temperature, $T = 293 \text{ K}$. The calculated MAE decreases as temperature rises, for example, $K_1 \sim 1.1 \text{ MJ/m}^3$ at 600 K [71]. Calculated Curie temperatures $T_c \sim 965 \text{ K}$ [71] and $T_c \sim 885 \text{ K}$ [74] compare well with experimental measurements $T_c \sim 920 \text{ K}$ [28] and $T_c \sim 987 \text{ K}$ [15]. KKRASA-CPA-DLM formalism has been applied to study temperature dependence of magnetization and the Curie temperature of the YCo_5 magnet doped by Ni and Fe [74]. Both experiments and calculations show an increase or a decrease in magnetization with Fe or Ni replacement, correspondingly. The same KKRASA-CPA-DLM formalism has been applied to study the temperature dependence of magnetization and MAE for the $Y(\text{Co}_{1-x-y}\text{Fe}_x\text{Cu}_y)_5$ magnets [81]. These calculations show that MAE of the YCo_5 magnet could be increased by adding relatively minor amounts of Fe and/or Cu, with the larger MAE field detected for the composition $Y(\text{Co}_{0.82}\text{Fe}_{0.09}\text{Cu}_{0.09})_5$ with the condition of a preferred replacement of Fe and Cu at 3g and 2c, correspondingly. The recent improvement of KKRASA-CPA-DLM methodology allowed Patrick and Staunton [82] to reproduce the experimental

MAE of the YCo_5 magnet, $K_1 \sim 5.0 \text{ MJ/m}^3$ [17], at room temperature. Recent overviews of the first-principles studies of the doped YCo_5 magnets are presented in refs. [83,84].

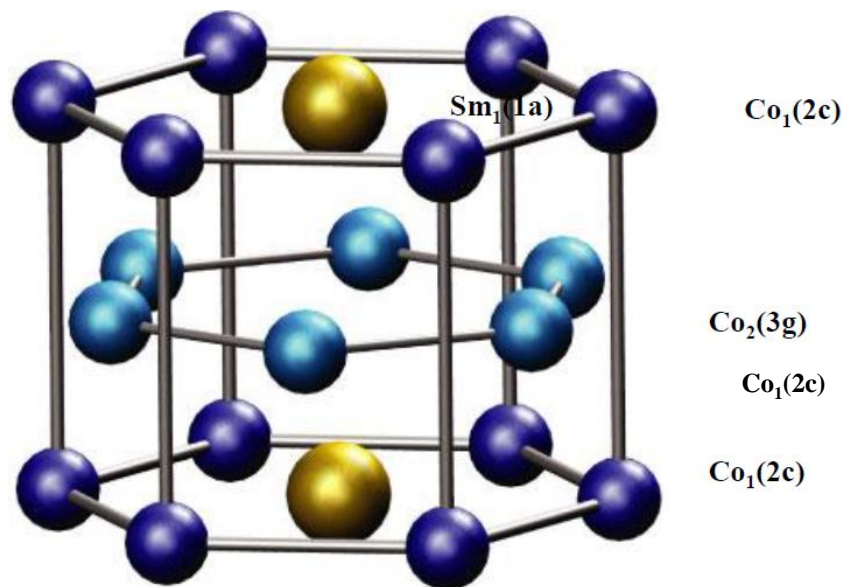


Figure 1. Crystal structure of SmCo_5 . The schematic is taken from ref. [62].

In addition to the numerous first-principle studies of the YCo_5 magnet, the phase stability and the thermodynamics of the Y-Co system have been assessed experimentally [85–87] and computationally, using the semi-empirical CALPHAD (CALculation of PHase Diagrams) method [88–90]. Experimentally, YCo_5 was reported to melt congruently at $T_m \sim 1623 \text{ K}$, possess a small homogeneity range at high temperature, and decompose below $T \sim 998 \text{ K}$ [86]. In addition, the Y-Co-Ni ternary system evaluation, reported by Gupta [91], revealed a complete solubility from YCo_5 to YNi_5 at 1073 K and 1273 K. This ternary system was assessed using the CALPHAD method [92,93], and the solubility of the $\text{Y}(\text{Co},\text{Ni})_5$ phase has been reproduced [92]. Experimental characterization of the Y-Co-Fe system demonstrated maximum solubility of Fe in $\text{Y}(\text{Co},\text{Fe})_5$ of $\sim 20 \text{ at.}\%$ [94] and $\sim 5 \text{ at.}\%$ [95] at 1323 K and 1073 K, correspondingly. There are no reported CALPHAD assessments (parameters) for Y-Co-Fe and Y-Fe-Ni ternary systems (a maximum solubility of $\sim 30 \text{ at.}\%$ Fe in $\text{Y}(\text{Fe},\text{Ni})_5$ was reported by [95] at 873 K), and no available information exists regarding thermodynamic properties or phase stability of the $\text{Y}(\text{Co},\text{Fe},\text{Ni})_5$ compound.

Therefore, the principal goal of the present research is to examine the stabilizing effects of adding nickel to the $\text{Y}(\text{Co}_{1-x}\text{Fe}_x)_5$ alloys. We employ *ab initio* calculations using two complementary techniques: (i) the fully relativistic exact muffin-tin orbital method (FREMTO) and (ii) the full-potential linear muffin-tin orbital method (FPLMTO). All methods account for all relativistic effects, the so-called spin-orbit coupling (SOC). The implementation of these particular methods ensures that our results are rigorous and independent of technical implementations while employing the most advantageous attributes and durability strengths of each method. Related details of the *ab initio* [96,97] and the CALPHAD computational methods are outlined in Section 2. Results of the density-functional-theory (DFT) calculations of the ground state properties of the $\text{Y}(\text{Co-Fe-Ni})_5$ alloys connected with CALPHAD calculations are outlined in Section 3. Next, we demonstrate results of the DFT calculations of the magnetic properties of the $\text{Y}(\text{Co-Fe-Ni})_5$ alloys in Section 4. Lastly, discussion and concluding remarks are outlined in Section 5.

2. Computational Methods

The calculations we denote as EMT0 are performed while using the Green's function formalism based on the improved screened Korringa–Kohn–Rostoker technique, where the one-electron potential

is defined by the optimized overlapping muffin-tin (OOMT) potential spheres [98,99]. Inside the potential spheres, the potential is spherically symmetric, while it is permanent between the spheres. The radius of the potential spheres, the spherical potential inside these spheres, and the permanent value in the interstitial region are resolved by minimizing (i) the deviation between the exact and overlapping potentials and (ii) the errors that are caused by the overlap between the spheres. Within the EMTO formalism, the one-electron states are calculated exactly for the OOMT potentials. As a product of the EMTO calculation, one can determine the self-consistent Green's function of the system and the complete, non-spherically symmetric charge density. Lastly, the total energy is calculated while using the full charge-density technique [100]. We consider, as the valence states, $6s$, $5p$, $5d$, and $4f$ states for Sm and $4s$ and $3d$ states for Co and Fe. The corresponding Kohn–Sham orbitals are expanded in terms of *spdf* exact muffin-tin orbitals, i.e., we select an orbital momentum cutoff $l_{max} = 3$. The EMTO orbitals, consequently, consist of the *spdf* partial waves (solutions of the radial Schrödinger equation for the spherical OOMT potential wells) and the *spdf* screened spherical waves (solutions of the Helmholtz equation for the OOMT muffin-tin zero potential). The completeness of the muffin-tin basis was discussed in detail in ref. [99]. The generalized gradient approximation (GGA-PBE) [101] is selected for the electron exchange and the correlation energy functional. Integration over the Brillouin zone is performed using the special k -point technique [102] with 784 k -points in the irreducible wedge of the zone (IBZ). The moments of the density of states, needed for the kinetic energy and valence charge density, are computed by integrating the Green's function over a complex energy contour with 2.2 Ry diameter while using a Gaussian integration technique with 30 points on a semi-circle enclosing the occupied states. In the case of the implementation of the FR-EMTO formalism, SOC is included through the four-component Dirac equation [103].

In order to treat compositional disorder, the EMTO method is coupled with the coherent potential approximation (CPA) [104,105]. The ground-state properties of the $Y(\text{Co}_{1-x-y}\text{Fe}_x\text{Ni}_y)_5$ alloys are obtained from EMTO-CPA calculations that include the Coulomb screening potential and energy [106–108]. The paramagnetic state of the $Y(\text{Co}_{1-x-y}\text{Fe}_x\text{Ni}_y)_5$ is modeled within the disordered local moment (DLM) approximation [109,110]. The equilibrium atomic density of the alloy is obtained from a Murnaghan fit to the total energy versus atomic volume curve [111].

The highest level of theory (least approximations) is implemented in a full-potential scheme, i.e., no structural approximations, which includes spin-orbit interaction as explained [112] for early and late lanthanides [96,113]. The full-potential linear muffin-tin orbital (FPLMTO) accomplishes this in ways that are detailed [114]. For Y, we use two energy parameters coupled with each basis function, and these parameters have different values for pseudocore states ($4s$ and $4p$) and valence states ($5s$, $5p$, $4d$, and $4f$). Test calculations including the $3d$ states as semi-core states for Y do not significantly change any result. For the TM atom, we use a similar set-up. The spin-orbit interaction and the orbital polarization (OP) operate on the d and f orbital. OP is introduced in FPLMTO in a self-consistent fashion so there are no fixed parameters. Because of the way it is constructed, the orbital polarization often enhances spin-orbit coupling, leading to better orbital moments [114]. Both the generalized gradient and the local-density approximations (GGA-PBE and LDA) [101,115] are applied.

For the computation of the magnetic anisotropy energy, i.e., the difference in total energy between spins pointing in plane (100) or perpendicular to the plane along the z axis (001), one finds small differences. To resolve these small numbers, one has to be very careful calculating the total energy for the two cases as consistent as possible. Here, we decide to remove all crystal symmetry, thus, from a symmetry set-up standpoint, the calculations are identical. This approach is less efficient but in practice more accurate because errors associated with different k points, Brillouin zones, and other numerical approximations are minimized. Brillouin zone integration over 10,000 k points is carried out using Fermi-Dirac broadening corresponding to room temperature.

The CALPHAD method permits the prediction of phase stability and thermodynamics of multi-component systems based on the extrapolation of the phase diagram data and the thermodynamic properties of its constitutive binary and ternary systems [116–118]. The CALPHAD formalism consists

of modeling Gibbs energy functions for each phase of the system (potentially including all elements) to reproduce the available thermodynamic (e.g., heat of formation) and phase diagram (e.g., melting point) data. Once the parameters of these functions are assessed for the constitutive systems, extrapolation (or prediction) can be made for multi-component systems. Here, we focus on heat of formation (thermodynamic property), phase diagram data (e.g., melting point, solubility limits), and CALPHAD assessment of the YTM_5 compound with $TM = Co, Fe, \text{ and } Ni$ as a first step toward the establishment of a complete $Y-Co-Fe-Ni$ database. Model parameters optimization and CALPHAD calculations are performed using the Thermo-Calc software package (2019b version) in combination with its PARROT module [119,120].

3. Thermodynamics Properties of the $Y(Co-Fe-Ni)_5$ Alloys

The YCo_5 compound crystallizes in the hexagonal $CaCu_5$ -type structure with three non-equivalent atomic sites: Y1-(1a), Co1-(2c), and Co2-(3g) (see Figure 1) with six atoms per formula unit and per computational cell.

Table 1 shows the equilibrium formula unit (f.u.) volume, bulk modulus, and the pressure derivative of the bulk modulus for the YCo_5 compound calculated using each of the ab initio techniques. The results of the EMTO calculations are presented both without (“SREMTO”, “SR” means scalar-relativistic) and with (“FREMTO”) inclusion of SOC. The experimental value of the equilibrium f.u. volume is taken from ref. [29,55]—see further discussion below. Notice that the equilibrium volume, calculated by FPLMTO method, agrees very well with the experimental data and that incorporating the relativistic SOC in the calculation has only a minor effect.

Table 1. Equilibrium formula unit volume, bulk modulus, and its pressure derivative of the YCo_5 compound as functions of the ab initio technique. The unit cell volume is measured at $T = 4.1$ K.

Property	SREMTO	FREMTO	FPLMTO	Expt. [29,55]
Unit cell volume (\AA^3)	85.07	85.24	82.65	82.50
c/a axial ratio			0.80	
Bulk modulus (GPa)	134.63	128.65	164	
Bulk modulus pressure derivative	3.70	3.81	2.62	

FPLMTO: full-potential linear muffin-tin orbitals.

Earlier neutron-diffraction studies of the $Th(Co_{1-x}Fe_x)_5$ alloys (also based on the $CaCu_5$ -type structure) [14] show that the larger Fe atoms preoccupies the 3g-type sites, whereas the smaller Co atoms choose to occupy the 2c-type sites. This occupational inclination has been affirmed by DFT calculations for YCo_5 [67] and $SmCo_5$ [68] compounds. In line with these calculations, the total energy for Fe at the 3g site (E_{3g}) is lower than for Fe at the 2c site (E_{2c}) by 0.21 eV/f.u. and 0.10 eV/f.u. for YCo_5 and $SmCo_5$ magnets, correspondingly. As was mentioned in refs. [19,28], if the YCo_5 magnet is doped with Fe and Ni, Fe atoms occupy preferentially 3g sites, while Ni atoms favor 2c sites.

Figure 2a shows the heat of formation calculated within the EMTO-CPA technique of the pseudo-binary $YFe_3(Ni_{1-x}Co_x)_2$ alloys where Fe atoms occupy all 3g-type sites and the occupation of the 2c-type sites continuously changes from pure Ni (the YFe_3Ni_2 compound) to pure Co (the YFe_3Co_2 compound). The current calculations show that the $YFe_3(Ni_{1-x}Co_x)_2$ alloys could remain stable until almost all Ni atoms are replaced by Co atoms.

For comparison, we also show (Figure 2b) the heat of formation calculated within the EMTO-CPA formalism [3,4] of the pseudo-binary $SmFe_3(Ni_{1-x}Co_x)_2$ alloys where Fe atoms occupy all 3g-type sites and the occupation of the 2c-type sites continuously changes from pure Ni (the $SmFe_3Ni_2$ compound) to pure Co (the $SmFe_3Co_2$ compound). These calculations show that the pseudo-binary $SmFe_3(Ni_{1-x}Co_x)_2$ alloys could remain stable until almost half of Ni atoms are replaced by Co atoms.

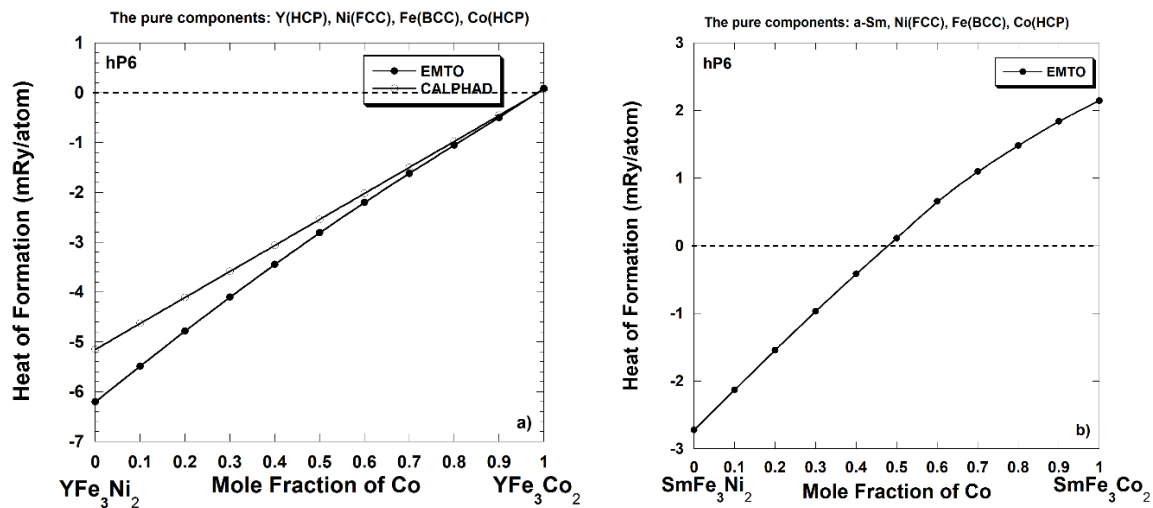


Figure 2. (a) The heat of formation of the pseudo-binary $\text{YFe}_3(\text{Ni}_{1-x}\text{Co}_x)_2$ alloys predicted via ab initio (0 K) and CALPHAD (298 K) calculations. (b) The heat of formation of the pseudo-binary $\text{SmFe}_3(\text{Ni}_{1-x}\text{Co}_x)_2$ alloys predicted via ab initio calculations [4].

In order to understand the difference between Figure 2a,b, one needs to take into consideration several of the following arguments. Nickel metal forms the stable CaCu_5 -type compounds with both yttrium and samarium metals. Calculated within EMTO formalism, the heat of formation of SmNi_5 and YNi_5 compounds (in the CaCu_5 -type structure) is -18.95 mRy/atom and -22.91 mRy/atom, correspondingly, which is in accord with the experimental measurements of -23.08 mRy/atom (-30.3 kJ/mole, SmNi_5 , [32]) and -25.98 mRy/atom (-34.1 kJ/mole, YNi_5 , [32]). As we mentioned in the Introduction, the YFe_5 compound as well as the SmFe_5 compound (see refs. [3,4]) do not exist in the equilibrium Y-Fe and Sm-Fe phase diagrams, correspondingly, thus no experimental information about the heat of formation of these hypothetical compounds is available. However, the EMTO calculations show that the heat of formation of the YFe_5 compound is positive, $+6.46$ mRy/atom, and is half of the calculated heat of formation of the SmFe_5 compound, $+12.68$ mRy/atom. As a result, the calculated heat of formation of the YFe_3Co_2 compound, $+0.09$ mRy/atom, appears to be smaller than the calculated heat of formation of the SmFe_3Co_2 compound, $+2.15$ mRy/atom [4]. The computed heats of formation of the YFe_3Ni_2 and the SmFe_3Ni_2 compounds are both negative (stable compounds), however, the absolute value of the calculated heat of formation of the YFe_3Ni_2 compound, $|-6.20|$ mRy/atom, is more than twice as high as the absolute value of the heat of formation of the SmFe_3Ni_2 compound, $|-2.72|$ mRy/atom [4]. As a result, the region of stability of the pseudo-binary $\text{YFe}_3(\text{Ni}_{1-x}\text{Co}_x)_2$ alloys appears to be almost twice as wide as the region of stability of the pseudo-binary $\text{SmFe}_3(\text{Ni}_{1-x}\text{Co}_x)_2$ alloys.

The promising phase stability of the YFe_3CoNi compound highlighted by the EMTO-predicted heat of formation of the pseudo-binary $\text{YFe}_3(\text{Ni}_{1-x}\text{Co}_x)_2$ alloys in Figure 2a sparks interest in studying the thermodynamics and the stability of the $\text{Y}(\text{Co,Fe,Ni})_5$ compounds versus temperature in the broader Y-Co-Fe-Ni composition space. As mentioned in Section 2, a full CALPHAD assessment of the Co-Fe-Ni-Y database requires evaluation of the constitutive binary (i.e., Co-Fe, Co-Ni, Co-Y, Fe-Ni, Fe-Y, Ni-Y) and ternary (i.e., Co-Fe-Ni, Y-Co-Fe, Y-Co-Ni, Y-Fe-Ni) systems. This study is focused on the Y-containing binary systems to leverage and confirm the ab initio findings and serve as foundation for an upcoming CALPHAD-centric study.

The first Y-Co CALPHAD assessment, in which all intermetallic compounds were evaluated as stoichiometric compounds, was reported by Du et al. [88]. This assessment was revisited in [89] to consider solubility range in YCo_5 and Y_2Co_{17} . As both structures of Y_2Co_{17} ($\text{Th}_2\text{Ni}_{17}$ -type structure at high temperature and $\text{Th}_2\text{Zn}_{17}$ -type structure at low temperature) are similar to the hexagonal CaCu_5 -type structure (YCo_5), Du and Lü [89] treated both Y_2Co_{17} and YCo_5 compounds as one phase

with the formula $(Y,Co)_1(Y,Co)_2Co_{15}$. The reasoning behind the use of a one-phase three-sublattice model is that homogeneity regions of Y_2Co_{17} and YCo_5 could be described by a $CaCu_5$ -type lattice in which part of the Ca sites is occupied by pairs of Co atoms [89]. However, as mentioned by Golumbfskie and Liu [90], modeling the YCo_5 and the Y_2Co_{17} compounds separately allows for the extension of this binary system to be more readily implemented into a multicomponent databases. Thus, YCo_5 and Y_2Co_{17} were modeled in [90] using $(Y,Co)_1(Co)_4(Co,Va)$ and $(Y,Co)_1(Y,Co)_2(Co)_{15}$ formulas, correspondingly. Note that vacancies (Va) were introduced, and first-principles calculations for the end members of the YCo_5 compound were used to parameterize the model. Finally, Golumbfskie and Liu [90] underlined that the Y_2Co_{17} phase should be produced via a congruent melting reaction (as experimentally accepted) rather than the result of the peritectic reaction (as produced by the assessment of [89]). The most recent assessment [90] was used as a starting point to re-assess the Y-Co phase diagram using simpler $(Y)_2(Co)_{17}$ and $(Y)_1(Co)_5$ two-sublattice models for Y_2Co_{17} and YCo_5 compounds, correspondingly, to ease the extension of the database to multicomponent systems while conserving the main features of the system.

The re-assessed Y-Co phase diagram is presented in Figure 3 (with model parameters reported in Table 2) and exhibits good agreement with experiments: (i) congruent melting of Y_2Co_{17} and YCo_5 at 1630 K (exp.: 1630 K [86]) and 1615 K (exp.: 1623 K [86]), correspondingly; (ii) decomposition temperature of YCo_5 at 914 K (exp.: ~998 K [86]); (iii) heat of formation of YCo_5 equal to -12.46 kJ/mole and -13.61 kJ/mole at 298 and 1000 K, correspondingly, compared with -12.20 ± 0.87 kJ/mole measured between 850 and 1200 K in [85]; (iv) heat of formation of Y_2Co_{17} equal to -8.74 kJ/mole and -9.47 kJ/mole at 298 and 1000 K, correspondingly, compared with -7.6 ± 0.80 kJ/mole measured between 850 and 1200 K in [8].

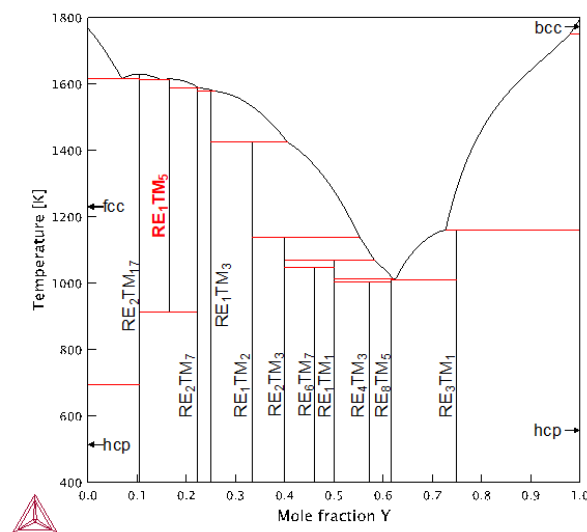


Figure 3. The Y-Co phase diagram calculated using the CALPHAD assessment presented in this study. Here, RE = Y and TM = Co.

The first CALPHAD assessment of the Y-Fe system was reported by Du et al. [121] and later refined by Lü et al. [122] to better replicate the ternary phase equilibria in the Y-Fe-Ni system. However, as mentioned by Konar et al. [123], the Gibbs energy of compounds reported in [121] was distinct from the experimental data, and neither the thermodynamic parameters for liquid or solid phases nor the invariant reactions were given in the updated assessment [122], making it impossible to evaluate. The Y-Fe system was re-assessed by Kardellass et al. [124,125] considering homogeneity range in the Y_6Fe_{23} and the YFe_2 phases compared to the stoichiometric compounds previously considered. Then, Konar et al. [123] published a new thermodynamic assessment of the Y-Fe system. However, the use of the modified quasichemical model for the liquid phase renders this work incompatible with the substitutional model used in other assessments. Thus, the latest assessment by Saenko et al. [126],

which is the most comprehensive and compatible one, is used in the present study. In addition to the four reported compounds (i.e., Y_2Fe_{17} , Y_6Fe_{23} , YFe_3 , YFe_2), we introduce the metastable YFe_5 compound based on the *ab initio* heat of formation (+6.46 mRy/atom = +8.48 kJ/mole). The introduction of this end-member in the $(Y)_1(Co,Fe,Ni)_5$ model (Table 2) does not change the Y-Fe phase diagram but permits us to calculate the heat of formation of $YFe_3(Ni_{1-x}Co_x)_2$ alloys when combined with the Y-Ni system.

Table 2. Optimized thermodynamic parameters of Y_2TM_{17} and YTM_5 compounds with TM = Co, Fe, Ni (J/mole).

Phase	Model	Reference
Y_2TM_{17}	Sublattice model: $(Co,Fe,Ni)_{17}(Y)_2$	
	$G_m^{Co_{17}Y_2} = -282934.050 + 44.6925387 \cdot T + 17^0 G_{Co}^{hcp} + 2^0 G_Y^{hcp}$	This work
	${}^0T_{c, Co:Y}^{Co_{17}Y_2} = +1167$	
	${}^0\beta_{Co:Y}^{Co_{17}Y_2} = +27.8$	
	$G_m^{Fe_{17}Y_2} = -237121 + 97 \cdot T + 17^0 G_{Fe}^{bcc} + 2^0 G_Y^{hcp}$	[126]
	${}^0T_{c, Co:Y}^{Fe_{17}Y_2} = +318$	
	${}^0\beta_{Co:Y}^{Fe_{17}Y_2} = +1.98$	
	$G_m^{Ni_{17}Y_2} = -386087 + 61.742 \cdot T + 17^0 G_{Ni}^{fcc} + 2^0 G_Y^{hcp}$	[121]
YTM_5	Sublattice model: $(Co,Fe,Ni)_5(Y)_1$	
	$G_m^{Co_5Y} = -117345.473 + 14.9230313 \cdot T + 5^0 G_{Co}^{hcp} + 0 G_Y^{hcp}$	This work
	$G_m^{Fe_5Y} = +5000 + 5^0 G_{Fe}^{bcc} + 0 G_Y^{hcp}$	This work
	$G_m^{Ni_5Y} = -186706 + 31.187 \cdot T + 5^0 G_{Ni}^{fcc} + 0 G_Y^{hcp}$	[121]

The Y-Ni system was assessed by Du and Zhang [127] considering all intermetallics as line compounds. This work was slightly modified by Mattern et al. [128] to reproduce Y-Nb-Ni data. Later on, Du and Lü [94] re-assessed the Y-Ni system to make it compatible with the three sublattice model used for the Y-Co assessment. This last work was also modified by Huang et al. [129] to fit the Y-Al-Ni system. Finally, Mezbahul-Islam and Medraj [130] assessed the Y-Ni system using the modified quasichemical model to consider the prevalence of short-range ordering in the liquid phase. In the present study, the initial assessment of Du and Zhang [127] is considered as it agrees with most experimental data [32,131,132]. In particular, the heat of formation of YNi_5 (−29.58 kJ/mole and −31.05 kJ/mole at 298 and 1000 K, correspondingly) [127] is in accord with the experimental data of −34.1 kJ/mole (298 K) [32] and -21.28 ± 0.42 kJ/mole (average between 887 and 1224 K) [131] and the calculated value of −30.09 kJ/mole (= −22.91 mRy/atom, present study).

The resulting CALPHAD model presented in Table 2 for the YTM_5 phase can now be used to calculate the heat of formation of the pseudo-binary $YFe_3(Ni_{1-x}Co_x)_2$ alloys with reference to hcp-Y, hcp-Co, bcc-Fe, and fcc-Ni at 298 K. As observed in Figure 2a, the CALPHAD results at 298 K are in excellent agreement with the *ab initio* predicted values at 0 K. Considering that the CALPHAD database is a combination from various sources (i.e., Y-Co re-assessed from [92], Y-Fe from [126] with new *ab initio* input, and Y-Ni from [127]), this agreement highlights both the predictive capability of *ab initio* methods and the flexibility and reliability of the CALPHAD method. The CALPHAD work performed in the present study on the Y-containing binary systems reveals a negative heat of formation across almost the entire $YFe_3(Ni_{1-x}Co_x)_2$ pseudo-binary, confirming the great potential of stabilizing a $YFe_3(Ni_{1-x}Co_x)_2$ magnet. However, additional assessments are required to include the experimental data gathered on the ternary Y-Co-Ni [91,95], Y-Fe-Ni [95], and Y-Co-Fe [94,95] systems to consistently represent the Gibbs energy landscape of the entire Y-Co-Fe-Ni composition space and propose alloy

compositions and thermal treatments to stabilize the Fe-rich $Y(\text{Co,Ni,Fe})_5$ magnet. The goal of the current paper is to examine the stabilizing outcomes (enthalpy) of adding nickel to the $Y(\text{Co}_{1-x}\text{Fe}_x)_5$ alloys and its impact on magnetic properties (Section 4); this additional CALPHAD work will be presented in a follow up paper.

4. Magnetic Properties of the $Y(\text{Co-Fe-Ni})_5$ Alloys

Table 3 presents the results of the FREMTO calculations of the site-projected spin, $m^{(s)}$, and orbital, $m^{(o)}$, moments of the $Y\text{Co}_5$ compound. According to [37], Y and Co spins should align in an antiparallel fashion (AF) that is predicted in the present self-consistent calculations. The calculated total moment, $m^{(tot)} = 7.82 \mu_B/\text{f.u.}$, is slightly smaller than the experimentally reported value of $8.30 \mu_B/\text{f.u.}$ [29]. The calculated spin moments are $1.55 \mu_B$ and $1.47 \mu_B$ for 2c and 3g sites, correspondingly, which are larger than the recorded experimental values of $1.44 \mu_B$ and $1.31 \mu_B$ [16,28]. The calculated orbital moments are $0.14 \mu_B$ and $0.11 \mu_B$ for 2c and 3g sites, correspondingly, which are smaller than recorded experimental data of $0.26 \mu_B$ and $0.24 \mu_B$ [16]. It is important to mention that the present FREMTO calculations reflect the experimental (spin flip-neutron scattering) observation; for the $Y\text{Co}_5$ compound, the orbital moment of $\text{Co}_1(2c)$ atoms is bigger than the orbital moment of $\text{Co}_2(3g)$ atoms [16,19,23,25], which was confirmed by the previous calculations [37,56,71]. The large MAE of the $Y\text{Co}_5$ compound comes from a big orbital allowance from $\text{Co}_1(2c)$ sites, which are located in the same plane as $Y_1(1a)$ sites [19,23,25]. Appropriately, $\text{Co}_1(2c)$ atoms have a big positive MAE allowance, while $\text{Co}_2(3g)$ atoms have a small negative MAE allowance. In line with ref. [71], the axial (positive) MAE of the $Y\text{Co}_5$ magnet can be achieved only if orbital moments on the $\text{Co}_1(2c)$ atoms are bigger than the orbital moments of the $\text{Co}_2(3g)$ atoms. The same outcome was reached in a past study [3,4]; in the SmCo_5 magnet, the orbital moment on $\text{Co}_1(2c)$ atom is bigger than on $\text{Co}_2(3g)$ atom. Calculations [3] anticipated MAE of the SmCo_5 magnet would be $K_1 = 19.63 \text{ MJ/m}^3$, which is actually close to the experimental data $K_1 = 17.2 \text{ MJ/m}^3$ [3].

Table 3. Site-projected spin, $m^{(s)}$, and orbital, $m^{(o)}$, magnetic moments for the $Y\text{Co}_5$ compound: FREMTO calculations. $m^{(tot)} = 7.82 \mu_B/\text{f.u.}$

Component:	$Y_1(1a)$	$Co_1(2c)$	$Co_2(3g)$
$m^{(s)} (\mu_B)$	+0.31	-1.55	-1.47
$m^{(o)} (\mu_B)$	-0.01	-0.14	-0.11

A mean-field treatment for the Curie temperature, T_c , can be formulated as [133,134]:

$$T_c = \frac{2}{3} \times \frac{E_{tot}^{DLM} - E_{tot}^{AF}}{k_B}$$

where $(E_{tot}^{DLM} - E_{tot}^{AF})$ is the difference among the ground state total energies of the DLM and the AF state, and k_B is the Boltzmann constant. Principally, an assessment of the Curie temperature can be achieved from the total energy difference between the ferromagnetic (or antiferromagnetic) and the paramagnetic states. However, in line with [133], the difference between the total energies can be substituted by the difference between the effective single-particle (one atomic specie) energies, which are directly associated with AF and DLM states (the so-called mean-field treatment). In the present work, E_{tot}^{DLM} and E_{tot}^{AF} are calculated at the equilibrium volumes for DLM and AF states, correspondingly. According to the present EMTO-DLM and EMTO-AF calculations, $T_c = 891.8 \text{ K}$ for the $Y\text{Co}_5$ magnet, which is in good accord with the experimental data $T_c = 920 \text{ K}$ [28], which is essentially bigger than that of the commonly used $\text{Nd}_2\text{Fe}_{14}\text{B}$ magnet ($T_c = 588 \text{ K}$ [7]). The similar EMTO calculations reveal $T_c = 1149.3 \text{ K}$ for the $Y\text{Fe}_5$ compound, although, as was mentioned in the Introduction, this compound does not exist in the Y-Fe phase diagram. However, as was also mentioned in the Introduction, there is an experimentally observed [42] tendency of the Curie temperature to increase with Fe doping of the

YCo₅ magnet, i.e., from $T_c = 930$ K (the YCo₅ compound) to $T_c = 1020$ K (the Y(Co_{0.8}Fe_{0.2})₅ compound). Our calculations qualitatively reflect this tendency.

Figure 4 shows the Curie temperature calculated within the EMTO-CPA technique of the pseudo-binary YFe₃(Ni_{1-x}Co_x)₂ alloys where Fe atoms occupy all 3g-type sites and the occupation of the 2c-type sites continuously changes from pure Ni (the YFe₃Ni₂ compound) to pure Co (the YFe₃Co₂ compound). The dotted line corresponds to the calculated Curie temperature of the YCo₅ magnet, $T_c = 891.8$ K. The calculated Curie temperature is equal to 572.6 K and 1097.7 K for the YFe₃Ni₂ and YFe₃Co₂ magnets, correspondingly. Although the calculated Curie temperature of the YFe₃Ni₂ compound lies about 320 K below of the Curie temperature of the YCo₅ magnet, this deficiency can be removed by substituting 70 at.% of Ni by Co. The Curie temperature of the YFe₃(Ni_{0.3}Co_{0.7})₂ magnet is equal to 899.9 K.

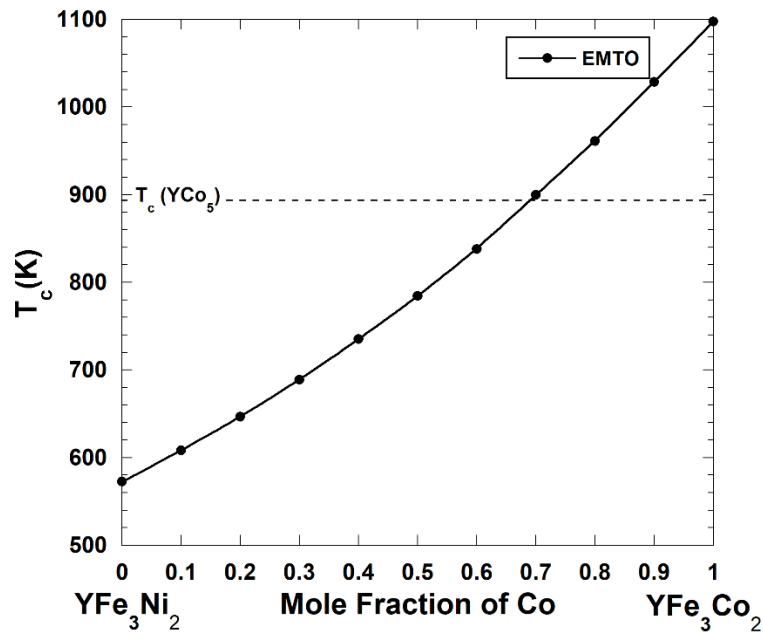


Figure 4. The Curie temperature of the pseudo-binary YFe₃(Ni_{1-x}Co_x)₂ alloys. The dotted line corresponds to the calculated Curie temperature of the YCo₅ magnet.

According to the present calculations, the YFe₃(Ni_{0.3}Co_{0.7})₂ magnet shows an enormous total moment of $m^{(tot)} \sim 9.79 \mu_B$, essentially due to the iron atoms that each contribute with $2.45 \mu_B$. The total moment of the YFe₃(Ni_{0.3}Co_{0.7})₂ magnet is thus essentially bigger than that of the traditional YCo₅ magnet that has a calculated total moment of $m^{(tot)} \sim 7.82 \mu_B$. The experimental values of saturation magnetization (M_s) and the maximum energy product ($(BH)_{max}$) for the YCo₅ magnet are 0.85 MA/m and 224 kJ/m³, correspondingly [6,10,11]. Because saturation magnetization and magnetic moment are approximately proportional, $M_s \sim m^{(tot)}$, and the maximum energy product is approximately proportional to the square of the saturation magnetization, $(BH)_{max} \sim (M_s)^2$ [135], one can evaluate that saturation magnetization for the YFe₃(Ni_{0.3}Co_{0.7})₂ magnet is proportional to:

$$M_s(YFe_3(Ni_{0.3}Co_{0.7})_2) \sim \frac{m^{(tot)}(YFe_3(Ni_{0.3}Co_{0.7})_2)}{m^{(tot)}(YCo_5)} \times M_s(YCo_5) \approx \frac{9.79}{7.82} \times 0.85 \frac{MA}{m} \approx 1.064 \frac{MA}{m}$$

and the maximum energy product for the YFe₃(Ni_{0.3}Co_{0.7})₂ magnet should be approximately:

$$(BH)_{max}(YFe_3(Ni_{0.3}Co_{0.7})_2) \sim \left(\frac{M_s(YFe_3(Ni_{0.3}Co_{0.7})_2)}{M_s(YCo_5)} \right)^2 \times (BH)_{max}(YCo_5) \approx 1.252^2 \times 224 \frac{kJ}{m^3} = 351 \frac{kJ}{m^3},$$

which is ~69% of the record maximum energy product of the Nd₂Fe₁₄B magnet, $(BH)_{max} = 512 \text{ kJ/m}^3$ [7]. Particularly, the YFe₃(Ni_{0.3}Co_{0.7})₂ magnet, which has a Curie temperature similar to the YCo₅ magnet, is a substantially steadier magnet than the YCo₅ magnet (its maximum energy product should be ~57% larger).

As has been mentioned in the Introduction, the magnetic anisotropy energy (MAE) is one of the more important properties of an efficient magnet. In the quest to increase the saturation magnetic moment or energy product, by substituting cobalt for iron, one has to review the impact of the doping on the MAE as well.

In Table 4 we collect calculated MAEs for the YCo₅-type magnets alloyed with iron, nickel, or both. Here, for the YFe₃Co₂ and the YFe₃CoNi magnets, we keep the iron atoms on the energetically favorably 3g sites as discussed above. In the case of YFe₃CoNi, we model Co and Ni on the 2c sites as two average atoms consistent with our modeling of SmFe₃CoNi [3]. In all calculations, we relax the atomic volume and the c/a axial ratio of the hexagonal phase. We find some sensitivity (not shown) of the MAE to the axial ratios, suggesting that the structural relaxation is important.

Table 4. FPLMTO results. GGA and LDA refer to generalized gradient approximation and local density approximation, correspondingly. K_1 reflects the magnetic anisotropy energy.

Material	Unit Cell Volume (Å ³)		c/a Ratio		K_1 (meV/cell)		K_1 (MJ/m ³)	
	GGA	LDA	GGA	LDA	GGA	LDA	GGA	LDA
YFe ₅	84.84	77.46	0.79	0.79	0.51	1.17	0.96	2.42
YCo ₅	82.65	76.38	0.80	0.80	9.89	6.44	19.17	13.51
YNi ₅	81.96	74.94	0.81	0.81	1.40	0.48	2.74	1.03
YFe ₃ Co ₂	86.40	77.28	0.79	0.79	2.01	6.71	3.73	13.91
YFe ₃ CoNi	86.22	76.38	0.81	0.82	4.51	5.04	8.38	10.57
YFe ₃ Ni ₂	86.34	76.64	0.84	0.83	1.93	3.69	3.58	7.69

According to the values calculated in Table 4, we realize that both YFe₅ and YNi₅ have relatively small magnetic anisotropy and, for that reason alone, they are not particularly good magnets. YFe₅ is really only included in the table to provide context to the other magnets, as it does not exist in the hexagonal phase. YCo₅ contrarily exists and is predicted to have significant magnetic anisotropy. We primarily rely on DFT-GGA calculations for these magnetic compounds because GGA performs better for the magnetic 3d transition metals relative to the LDA or even more modern approximations [136]. It is also a well-known fact that GGA reproduces the proper magnetic ground state of iron, as opposed to the LDA. Our GGA calculations reproduce the experimental atomic volume very well but overestimate the MAE for YCo₅ relative to experimental data. DFT-GGA ($T = 0 \text{ K}$) gives the unit cell volume $V_{cell} = 82.65 \text{ Å}^3$ and anisotropy $K_1 = 9.89 \text{ meV/cell}$ (19.2 MJ/m^3). These numbers shall be compared to experimental data at $T = 4.1 \text{ K}$, $V_{cell} = 82.50 \text{ Å}^3$ [29,55], $K_1 = 3.80 \text{ meV/cell}$ (7.38 MJ/m^3) [29,56] and at $T = 293 \text{ K}$, $V_{cell} = 83.99 \text{ Å}^3$ [33], $K_1 = 3.04 \text{ meV/cell}$ (5.80 MJ/m^3) [29,56]. Here, the unit cell volume at $T = 4.1 \text{ K}$, $V_{cell} = 82.50 \text{ Å}^3$ is identified using the experimental value of the MAE coefficient, K_1 , presented in the units of (MJ/m^3), [29,56], and (meV/cell) [55]. Steinbeck et al. [56], on the other hand, calculated $K_1 = 4.4 \text{ meV/cell}$ using LDA and orbital polarization in better agreement with experimental data. However, their calculation was performed at the experimental cell volume and not the LDA volume, which is drastically smaller. Their agreement with experiment is thus somewhat coincidental. We believe the difference in the calculated K_1 numbers is mostly due to electron exchange and correlation approximation. In Table 4, we also show our LDA results, and for YCo₅ (6.44 meV/cell), it is closer to experimental data (3.8 meV/cell) [29,55] than our GGA result.

Unfortunately, we realize that the MAE for these magnetic systems can be very sensitive to the particular DFT approximation (GGA or LDA) that is applied. Furthermore, there does not appear to be a simple systematic explanation for the difference in the MAE when comparing GGA and LDA

methods. The results are very consistent for YFe_5 , YNi_5 (small MAE), and YFe_3CoNi (intermediate MAE $\sim 4.5\text{--}5$ meV/cell), while for YCo_5 , the GGA produces a value significantly greater than the LDA (9.89 and 6.44 meV/cell, correspondingly). For YFe_3Co_2 and YFe_3Ni_2 , the LDA values are about three and two times larger than the GGA number, correspondingly. Apparently, the particular electron exchange and the correlation approximation are important for the anisotropy, and to explore this further, we applied several other popular formulations for YFe_3Co_2 ; the resulting MAE varied very sensitively. This remarkable sensitivity has not been recognized before for these types of magnets and certainly warrants further studies.

5. Discussion and Conclusions

According to our past calculations [3,4], replacing most of Co with Fe in the SmCo_5 magnet and using Ni as a thermodynamic mediator results in an SmFe_3CoNi magnet that has extraordinary magnetic properties, such as a very high Curie temperature, robust magnetic anisotropy about twice that of the $\text{Nd}_2\text{Fe}_{14}\text{B}$ magnet, and a big maximum energy product (an estimated 70.5% of the record maximum energy product of the $\text{Nd}_2\text{Fe}_{14}\text{B}$ magnet), which should be about 56% larger than that of the SmCo_5 precursor. However, even if we substitute a relatively expensive metal Co (283 RMB/kg) by cheaper Ni (99 RMB/kg) and Fe (3 RMB/kg), the cost of the suggested SmFe_3CoNi magnet is still mostly defined by the relatively expensive RE samarium metal (450 RMB/kg). Thus, in this paper, we expand on the fundamental idea of refs. [3,4] by using nickel metal as the stabilizing material in the YCo_5 magnet (Y is almost half the price of Sm [5]) in order to accommodate the maximum amount of iron metal to favor a very high magnetization.

We find a significant difference between the regions of stability of the $\text{YFe}_3(\text{Ni}_{1-x}\text{Co}_x)_2$ and $\text{SmFe}_3(\text{Ni}_{1-x}\text{Co}_x)_2$ alloys. In order to stabilize the $\text{SmFe}_3(\text{Ni}_{1-x}\text{Co}_x)_2$ alloys, one should have at least half of the 2c-type sites to be occupied by Ni atoms. The extreme case is the SmFe_3CoNi magnet, where Fe atoms occupy all 3g-type sites, and Ni and Co atoms occupy the 2c-type sites with equal probability, which has been suggested in refs [3,4]. For the $\text{YFe}_3(\text{Ni}_{1-x}\text{Co}_x)_2$ alloys, it is possible to have the stable solutions until approximately all Ni atoms are substituted by Co atoms. Our ab initio heat of formation predictions are confirmed by CALPHAD modeling at 298 K (Figure 2a). The combination of negative heat of formation and extended solubility limits experimentally observed in the YTM_5 ($\text{TM} = \text{Co}, \text{Fe}, \text{Ni}$) magnets (i.e., complete solubility from YCo_5 to YNi_5 at 1073 K and 1273 K; solubility of ~ 20 at.% Fe in $\text{Y}(\text{Co},\text{Fe})_5$ at 1323 K [94]; solubility of ~ 30 at.% Fe in $\text{Y}(\text{Fe},\text{Ni})_5$ at 873 K [95]) is promising for experimentalists who would like to synthesize these new magnets. Based on a thorough literature review, theoretical calculations, and preliminary CALPHAD works presented in this study, an in-depth CALPHAD assessment of the Y-Co-Fe-Ni system has been initiated and will provide guidance on how to make these new magnets. Meanwhile, a specific example from this work is the YFe_3Co_2 magnet for which we calculated the Curie temperature, T_c , which is equal to 1097.7 K and the maximum energy product, $(BH)_{\max}(\text{YFe}_3\text{Co}_2)$, as ~ 365 kJ/m³, which is $\sim 71\%$ of the record maximum energy product of the $\text{Nd}_2\text{Fe}_{14}\text{B}$ magnet, $(BH)_{\max} = 512$ kJ/m³. Here, the maximum energy products of YFe_3Co_2 and YFe_3CoNi magnets are estimated using the calculated total magnetic moments of YFe_3Co_2 , YFe_3CoNi , and YCo_5 magnets as well as the experimental values of the saturated magnetization and the maximum energy product of the YCo_5 magnet. Calculations are performed in the same fashion as for the $\text{YFe}_3(\text{Ni}_{0.3}\text{Co}_{0.7})_2$ magnet (see Section 4).

According to our calculations, the $\text{YFe}_3(\text{Ni}_{0.3}\text{Co}_{0.7})_2$ magnet has a Curie temperature $T_c \sim 900$ K that is relatively close to the calculated Curie temperature of the YCo_5 magnet, $T_c \approx 892$ K. In addition, the maximum energy product of the $\text{YFe}_3(\text{Ni}_{0.3}\text{Co}_{0.7})_2$ magnet is significantly improved compared to the YCo_5 magnet ($\sim 57\%$ larger).

The calculated intrinsic properties of the magnets suggested in ref. [3,4] and in this paper are reported in Table 5 in conjunction with the experimental data of $\text{Nd}_2\text{Fe}_{14}\text{B}$, SmCo_5 , and YCo_5 magnets for comparison. All four suggested permanent magnets have a Curie temperature significantly higher than that of the Neomax ($\text{Nd}_2\text{Fe}_{14}\text{B}$), $T_c \approx 588$ K, spanning from 785 K to 1103 K. In addition,

their maximum energy products are significantly higher than that of the commercially used SmCo₅ and YCo₅ magnets (231 kJ/m³ and 224 kJ/m³, correspondingly), reaching a maximum value of 365 kJ/m³ for YFe₃Co₂. Our calculated (Table 4, LDA) MAEs for YFe₃CoNi magnet is not much smaller than that of YCo₅ magnet (10.6 MJ/m³ and 13.5 MJ/m³, correspondingly).

Table 5. Intrinsic magnetic properties of Nd₂Fe₁₄B, SmCo₅, and YCo₅ (experiment [6,7,10,11]); and SmFe₃CoNi [3,4], YFe₃CoNi, (K₁, LDA), YFe₃(Ni_{0.3}Co_{0.7})₂, and YFe₃Co₂ (theory) permanent magnets.

Material	M_s (MA/m)	T_c (K)	K_1 (MJ/m ³)	$ BH _{max}$ (kJ/m ³)
Nd ₂ Fe ₁₄ B	1.28	588	4.9	512
SmCo ₅	0.86	1020	17.2	231
YCo ₅	0.85	987	6.5	224
SmFe ₃ CoNi	1.08	1103	9.2	361
YFe ₃ CoNi	1.00	785	10.6	309
YFe ₃ (Ni _{0.3} Co _{0.7}) ₂	1.06	900		351
YFe ₃ Co ₂	1.14	1098		365

Although the cobalt price plunged from more than 630 RMB/kg (May 2018) to 282 RMB/kg (June 2020) during the last two years, it is unlikely it will reach its record low value of approximately 157 RMB/kg (June 2016) as the global electric car market (production) continues to grow at an accelerated pace. Indeed, cobalt remains a necessary component in electric vehicle lithium-ion batteries, e.g., LiCoO₂, and cobalt costs will probably rise as a result of anticipated demands for lithium-ion batteries, which consume more than 70% of total cobalt mining. Considering SmFe₃CoNi and YFe₃CoNi magnets comprise 80% less Co than their SmCo₅ and YCo₅ precursors, maturing of these magnets becomes even more captivating from the current economic viewpoint.

In conclusion, we showed that replacing part of cobalt with iron in SmCo₅ and YCo₅ magnets stabilized with a small portion of nickel results in novel permanent magnets that we consider to be conceivably synthesized. They are anticipated to have outstanding magnetic properties, a big maximum energy product, a strong magnetic anisotropy, and an exceptionally high Curie temperature. However, it is very important to emphasize that, although these three intrinsic parameters are necessary to be large for an efficient permanent magnet, this is not a sufficient condition. It is also necessary to optimize the microstructure of the alloys in order to optimize the extrinsic magnetic properties.

Author Contributions: Conceptualization, A.L.; methodology, A.L., P.S., A.P., E.E.M.; writing-review and editing, A.L., P.S., A.P., E.E.M. All authors have read and agreed to the published version of the manuscript.

Funding: This research is supported by the Critical Materials Institute, an Energy Innovation Hub funded by the US Department of Energy, Office of Energy Efficiency and Renewable Energy, Advanced Manufacturing Office.

Acknowledgments: The work is performed under the auspices of the US Department of Energy by the Lawrence Livermore National Laboratory under Contract No. DE-AC52-07NA27344. A.L. thanks A. Ruban, O. Peil, P. Korzhavyi, and L. Vitos for technical support. A.P. and A.L. thank the dedication, responsiveness, and expertise of the staff of the LLNL Research Library.

Conflicts of Interest: The authors declare no conflict of interest.

References

1. Buschow, K.H.J. New developments in hard magnetic materials. *Rep. Prog. Phys.* **1991**, *54*, 1123–1214. [[CrossRef](#)]
2. Buschow, K.H.J.; de Boer, F.R. *Physics of Magnetism and Magnetic Materials*; Kluwer Academic/Plenum: New York, NY, USA, 2004.

3. Söderlind, P.; Landa, A.; Loch, I.L.M.; Åberg, D.; Kvashnin, Y.; Pereiro, M.; Däne, M.; Turchi, P.E.A.; Antropov, V.P.; Eriksson, O. Prediction of the new efficient permanent magnet SmCoNiFe_3 . *Phys. Rev. B* **2017**, *96*, 100404-1–100404-5(R). [[CrossRef](#)]
4. Landa, A.; Söderlind, P.; Parker, D.; Åberg, D.; Lordi, V.; Perron, A.; Turchi, P.E.A.; Chouhan, R.K.; Paudyal, D.; Lograsso, T.A. Thermodynamics of SmCo_5 compound doped with Fe and Ni: An ab initio study. *J. Alloy. Compd.* **2018**, *765*, 659–663. [[CrossRef](#)]
5. Zhang, D.-T.; Cai, N.-X.; Zhu, R.-C.; Liu, W.-Q.; Yue, M. Low-cost $\text{Sm}_{0.7}\text{Y}_{0.3}\text{Co}_5$ sintered magnet produced by traditional powder metallurgical techniques. *Rare Met.* **2019**, *39*, 421–428. [[CrossRef](#)]
6. Coey, J.M.D. Permanent magnets: Plugging the gap. *Scr. Mater.* **2012**, *67*, 524–529. [[CrossRef](#)]
7. Coey, J.M.D. Hard magnetic materials: A Perspective. *IEEE Trans. Magn.* **2011**, *47*, 4671–4681. [[CrossRef](#)]
8. Gutfleisch, O.; Willard, M.A.; Brück, E.; Chen, C.H.; Sankar, S.G.; Liu, J.P. Magnetic materials, and devices for the 21st century: Stronger, lighter, and more energy efficient. *Adv. Mater.* **2011**, *23*, 821–842. [[CrossRef](#)]
9. Kramer, M.J.; McCallum, R.W.; Anderson, I.A.; Constantinides, S. Prospects for non-rare earth permanent magnets for traction motors and generators. *JOM* **2012**, *64*, 752–763. [[CrossRef](#)]
10. Hoffer, G.; Strnat, K. Magnetocrystalline anisotropy of YCo_5 and Y_2Co_{17} . *IEEE Trans. Magn.* **1966**, *2*, 487–489. [[CrossRef](#)]
11. Strnat, K.; Hoffer, G.; Olson, J.; Ostertag, W. A Family of new cobalt-base permanent magnet materials. *J. Appl. Phys.* **1967**, *38*, 1001–1002. [[CrossRef](#)]
12. Strnat, K.J. The recent development of permanent magnet materials containing rare earth metals. *IEEE Trans. Magn.* **1970**, *6*, 182–189. [[CrossRef](#)]
13. Buschow, K.H. Composition and stability of CaCu_5 -type compounds of yttrium with iron and cobalt. *J. Less-Common Met.* **1973**, *31*, 359–364. [[CrossRef](#)]
14. Laforest, J.; Shan, J.S. Neutron diffraction study of the $\text{Th}(\text{Co}_{1-x}\text{Fe}_x)_5$ alloys. *IEEE Trans. Magn.* **1973**, *9*, 217–220. [[CrossRef](#)]
15. Klein, H.P.; Menth, A.; Perkins, R.S. Magnetocrystalline anisotropy of light rare-earth cobalt compounds. *Physica B+C* **1975**, *80*, 153–163. [[CrossRef](#)]
16. Heidemann, A.; Richter, R.; Buschow, K.H.J. Investigation of the hyperfine fields in the compounds LaCo_{13} , LaCo_5 , YCo_5 and ThCo_5 by means of inelastic neutron scattering. *Eur. Phys. J. B* **1975**, *22*, 367–372. [[CrossRef](#)]
17. Ermolenko, A.S. Magnetocrystalline anisotropy of rare earth intermetallics. *IEEE Trans. Magn.* **1976**, *12*, 992–996. [[CrossRef](#)]
18. Déportes, J.; Givord, D.; Lemaire, R.; Nagai, H.; Yang, Y.T. Influence of substitutional pairs of cobalt atoms on the magnetocrystalline anisotropy of cobalt-rich rare-earth compounds. *J. Less-Common Met.* **1976**, *44*, 273–279. [[CrossRef](#)]
19. Déportes, J.; Givord, D.; Schweizer, J.; Tasset, F. Different contributions of the two cobalt sites to the magnetocrystalline anisotropy of YCo_5 and related compounds. *IEEE Trans. Magn.* **1976**, *12*, 1000–1002. [[CrossRef](#)]
20. Buschow, K.H.J. Intermetallic compounds of rare-earth and 3d transition metals. *Rep. Prog. Phys.* **1977**, *40*, 1179–1256. [[CrossRef](#)]
21. Malik, S.K.; Arlinghaus, F.A.; Wallace, W.E. Spin-polarized energy-band structure of YCo_5 , SmCo_5 , and GdCo_5 . *Phys. Rev. B* **1977**, *16*, 1242–1248. [[CrossRef](#)]
22. Kirchmayr, H.R.; Poldy, C.A. Magnetism in rare earth—3d intermetallics. *J. Magn. Magn. Mater.* **1978**, *8*, 1–42. [[CrossRef](#)]
23. Streever, R.L. NMR investigation of Co magnetic anisotropy in RCo_5 compounds. *Phys. Lett. A* **1978**, *65*, 360–362. [[CrossRef](#)]
24. Alameda, J.M.; Déportes, J.; Givord, D.; Lemaire, R.; Lu, Q. Large magnetization anisotropy in uniaxial YCo_5 intermetallic. *J. Magn. Magn. Mater.* **1980**, *15–18*, 1257–1258. [[CrossRef](#)]
25. Streever, R.L. Individual Co site contributions to the magnetic anisotropy of RCo_5 compounds and related structures. *Phys. Rev. B* **1979**, *19*, 2704–2711. [[CrossRef](#)]
26. Wohlfarth, E.P. First and second order transitions in some metallic ferromagnets. *J. Appl. Phys.* **1979**, *50*, 7542–7544. [[CrossRef](#)]
27. Wohlfarth, E.P. The Curie temperatures of compounds of the heavy rare earths and yttrium with cobalt. *J. Phys. F Met. Phys.* **1979**, *9*, L123–L128. [[CrossRef](#)]

28. Schweitzer, J.; Tasset, F. Polarized neutron study of the RCo₅ intermetallic compounds. I. The cobalt magnetization in YCo₅. *J. Phys. F Met. Phys.* **1980**, *10*, 2799–2817. [[CrossRef](#)]
29. Alameda, J.M.; Givord, D.; Lemaire, R.; Lu, Q. Co energy and magnetization anisotropies in RCo₅ intermetallics between 4.2 K and 300 K. *J. Appl. Phys.* **1981**, *52*, 2079–2081. [[CrossRef](#)]
30. Inomata, K. Individual Co site contributions to the magnetic anisotropy and NMR investigation of Y₂(Co_{1-x}M_x)₁₇ (M=Cu,Al). *Phys. Rev. B* **1981**, *23*, 2076–2081. [[CrossRef](#)]
31. Chuang, Y.C.; Wu, C.H.; Chang, Y.C. Structure and magnetic properties of Y(Co_{1-x}M_x)₅ compounds. *J. Less Common Met.* **1982**, *84*, 201–213. [[CrossRef](#)]
32. Pasturel, A.; Colinet, C.; Allibert, C.; Hicter, P.; Percheron-Guegan, A.; Achard, J.C. A Theoretical and Experimental Study of the Enthalpies of Formation of LaNi₅-Type Compounds. *Phys. Status Solidi B* **1984**, *125*, 101–106. [[CrossRef](#)]
33. Meyer-Liautaud, F.; Derkaout, S.; Allibert, C.H.; Castanet, R. Structural and thermodynamic data on the pseudobinary phases R(Co_{1-x}Cu_x)₅ WITH R ≡ Sm, Y, Ce. *J. Less Common Met.* **1987**, *127*, 231–242. [[CrossRef](#)]
34. Franse, J.J.M.; Thuy, N.P.; Hong, N.M. Individual site magnetic anisotropy of the iron and cobalt ions in rare earth-iron and rare earth-cobalt intermetallic compounds. *J. Magn. Magn. Mater.* **1988**, *72*, 361–366. [[CrossRef](#)]
35. Strnat, K.J.; Strnat, R.M.W. Rare earth-cobalt permanent magnets. *J. Magn. Magn. Mater.* **1991**, *100*, 38–56. [[CrossRef](#)]
36. Zhao, T.-S.; Jin, H.-M.; Gua, G.-H.; Han, X.-F.; Chen, H. Magnetic properties of R ions in RCo₅ compounds (R=Pr, Nd, Sm, Gd, Tb, Dy, Ho, and Er). *Phys. Rev. B* **1991**, *43*, 8593–8598. [[CrossRef](#)]
37. Nordström, L.; Brooks, M.S.S.; Johansson, B. Calculation of orbital magnetism and magnetocrystalline anisotropy energy in YCo₅. *J. Phys. Condens. Matter* **1992**, *4*, 3261–3272. [[CrossRef](#)]
38. Coehoorn, R.; Daalderop, G.H.O. Magnetocrystalline anisotropy in new magnetic materials. *J. Magn. Magn. Mater.* **1992**, *104–107*, 1081–1085. [[CrossRef](#)]
39. Daalderop, G.H.O.; Kelly, P.J.; Schuurmans, M.F.H. Magnetocrystalline anisotropy of RECo₅ compounds. *J. Magn. Magn. Mater.* **1992**, *104–107*, 737–738. [[CrossRef](#)]
40. Trygg, J.; Nordström, L.; Johansson, B. First-principles calculations of the magnetocrystalline anisotropy energy for the pseudobinary compound. In *Physics of Transition Metals*; Oppeneer, P.M., Kübler, J., Eds.; Publisher World Scientific: Singapore, 1993; pp. 745–748.
41. Radwanski, R.J.; Franse, J.J.M. Magnetic properties of the 3d sublattice in R_nT_m intermetallics. *Int. J. Mod. Phys.* **1993**, *7*, 782–785. [[CrossRef](#)]
42. Paoluzi, A.; Pareti, L.; Solzi, M.; Albertini, F. Study of the iron contribution to the 3d-sublattice anisotropy in some uniaxial YCoFe structures derived from the CaCu₅ unit cell. *J. Magn. Magn. Mater.* **1994**, *132*, 185–190. [[CrossRef](#)]
43. Colinet, C. The thermodynamic properties of rare earth metallic systems. *J. Alloy. Compd.* **1995**, *225*, 409–422. [[CrossRef](#)]
44. Crisan, V.; Popescu, V.; Vernes, A.; Andreica, D.; Burda, I.; Cristea, S. On the electronic properties of YCo_{5-x}Ni_x. *J. Alloy. Compd.* **1995**, *223*, 147–150. [[CrossRef](#)]
45. Daalderop, G.H.O.; Kelly, P.J.; Schuurmans, M.F.H. Magnetocrystalline anisotropy of YCo₅ and related RECo₅ compounds. *Phys. Rev. B* **1996**, *53*, 14415–14433. [[CrossRef](#)] [[PubMed](#)]
46. Yamaguchi, M.; Asano, S. First-principles calculation of the 3d magnetocrystalline anisotropy energy of YCo₅. *J. Appl. Phys.* **1996**, *79*, 5952–5954. [[CrossRef](#)]
47. Yamaguchi, M.; Asano, S. First-principles calculations of the 3d magnetocrystalline anisotropy energy of YCo₅, Y₂Co₇, YCo₃, and Y₂Co₁₇. *J. Magn. Magn. Mater.* **1997**, *168*, 161–168. [[CrossRef](#)]
48. Kitagawa, I.; Terao, K.; Aoki, M.; Yamada, H. Electronic structure, and magnetism of YCo₅, YNi₅, and YCo₃Ni₂. *J. Phys. Condens. Matter* **1997**, *9*, 231–239. [[CrossRef](#)]
49. Zhang, G.W.; Feng, Y.P.; Ong, C.K. Electronic and magnetic properties of intermetallic compound YCo₅. *J. Magn. Magn. Mater.* **1998**, *184*, 215–221. [[CrossRef](#)]
50. Gratz, E.; Lindbaum, A.; Markosyan, A.S.; Milnera, M. Magnetoresistance in Y(Ni_{1-x}Co_x)₅ around the critical concentration for the onset of ferromagnetism. *J. Magn. Magn. Mater.* **1998**, *184*, 372–374. [[CrossRef](#)]
51. Yamada, H.; Terao, K.; Ishikawa, F.; Yamaguchi, Y.; Mitamura, H.; Goto, T. Itinerant-electron metamagnetism of Y(Co,Ni)₅. *J. Phys. Condens. Matter* **1999**, *11*, 483–492. [[CrossRef](#)]

52. Maruyama, F.; Nagai, H.; Amako, Y.; Yoshie, H.; Adachi, K. Magnetic properties of the hypothetical compound YFe_5 . *Physica B* **1999**, *266*, 356–360. [[CrossRef](#)]
53. Téllez-Blanco, J.C.; Grössinger, R.; Sato Turtelli, R.; Estévez-Rams, E. Magnetic and Structural Properties of $YCo_{5-x}Cu_x$. *IEEE Trans. Magn.* **2000**, *36*, 3333–3335. [[CrossRef](#)]
54. Al-Omari, I.A.; Skomski, R.; Thomas, R.A.; Lieslie-Pelesky, D.; Sellmyer, D.J. High-temperature magnetic properties of mechanically alloyed $SmCo_5$ and YCo_5 magnets. *IEEE Trans. Magn.* **2001**, *37*, 2534–2536. [[CrossRef](#)]
55. Steinbeck, L.; Richter, M.; Eschrig, H. Magnetocrystalline anisotropy of RCo_5 intermetallics: Itinerant-electron contribution. *J. Magn. Magn. Mater.* **2001**, *226–230*, 1011–1013. [[CrossRef](#)]
56. Steinbeck, L.; Richter, M.; Eschrig, H. Itinerant-electron magnetocrystalline anisotropy energy of YCo_5 and related compounds. *Phys. Rev. B* **2001**, *63*, 184431-1–184431-14. [[CrossRef](#)]
57. Kashyap, A.; Skomski, R.; Sabiryanov, R.R.F.; Jaswal, S.S.; Sellmyer, D.J. Exchange interactions and Curie temperature of Y-Co compounds. *IEEE Trans. Magn.* **2003**, *39*, 2908–2910. [[CrossRef](#)]
58. Larson, P.; Mazin, I.I. Calculation of magnetic anisotropy energy in YCo_5 . *J. Magn. Magn. Mater.* **2003**, *264*, 7–13. [[CrossRef](#)]
59. Larson, P.; Mazin, I.I. Magnetic properties of $SmCo_5$ and YCo_5 . *J. Appl. Phys.* **2003**, *93*, 6888–6890. [[CrossRef](#)]
60. Larson, P.; Mazin, I.I.; Papaconstantopoulos, D.A. Effects of doping on the magnetic anisotropy energy in $SmCo_{5-x}Fe_x$ and $YCo_{5-x}Fe_x$. *Phys. Rev. B* **2004**, *69*, 134408-1–134408-7. [[CrossRef](#)]
61. Larson, P.; Mazin, I.I. Effect of impurities on magnetic properties of $Y(Co_{5-x}Cu_x)$ and $Y_2(Co_{7-x}Ni_x)$. *J. Magn. Magn. Mater.* **2004**, *269*, 176–183. [[CrossRef](#)]
62. Rosner, N.; Koudela, D.; Schwarz, U.; Handstein, A.; Hafland, M.; Opahle, I.; Koepnik, K.; Kuz'min, M.D.; Müller, K.-H.; Mydosh, J.A.; et al. Magneto-elastic lattice collapse in YCo_5 . *Nat. Phys.* **2006**, *2*, 469–472. [[CrossRef](#)]
63. Wu, Q.; Chen, Z.; Xu, G.; Lu, X.; Zhong, K.; Huang, Z. Effects of doping on magnetic properties of $YCo_{5-x}Fe_x$ and $YCo_{5-x}Ag_x$ —First Principles Calculation. *J. Rare Earths* **2006**, *24* (Suppl. 1), 293–297. [[CrossRef](#)]
64. Koudela, D.; Schwarz, U.; Rosner, H.; Burkhardt, U.; Handstein, A.; Hanfland, M.; Kuz'min, M.D.; Opahle, I.; Koepnik, K.; Müller, K.-H.; et al. Magnetic and elastic properties of YCo_5 and $LaCo_5$ under pressure. *Phys. Rev. B* **2008**, *77*, 024411-1–024411-7. [[CrossRef](#)]
65. Castillo, M.C.G.; Aquino, J.A.M. Magnetic and electronic properties of the compound $Y(Co,Fe)_5$ calculated by the augmented spherical wave method. *Adv. Mater. Res.* **2009**, *68*, 145–151.
66. Colin, C.V.; Isnard, O.; Guillot, M. High magnetic field study of the anisotropy and neutron diffraction investigation of the crystal and magnetic structure of YCo_4 . *5Ge0.5*. *J. Alloy. Compd.* **2010**, *505*, 11–16. [[CrossRef](#)]
67. Liu, X.B.; Altounian, Z.; Yue, M. Effect of Fe partial substitution for Co on the magnetic properties of $Y(Co,Fe)_5$ from first-principles. *J. Appl. Phys.* **2010**, *107*, 09A718-1–09A718-3. [[CrossRef](#)]
68. Liu, X.B.; Altounian, Z. Magnetic moments and exchange interaction in $Sm(Co, Fe)_5$ from first-principles. *Comput. Mater. Sci.* **2011**, *50*, 841–846. [[CrossRef](#)]
69. Ohashi, K. Present and future of Sm_2Co_{17} magnets. *J. Jpn. Inst. Met.* **2012**, *76*, 96–106. [[CrossRef](#)]
70. Zhu, J.-X.; Janoscheck, M.; Rosenberg, R.; Ronning, F.; Thomson, J.D.; Torrez, M.; Bauer, E.D.; Bastia, C.D. LDA+DMFT approach to magnetocrystalline anisotropy of strong magnets. *Phys. Rev. X* **2014**, *4*, 021027-1–021027-7. [[CrossRef](#)]
71. Matsumoto, M.; Banerjee, R.; Staunton, J.B. Improvement of magnetic hardness at finite temperatures: Ab initio disordered local-moment approach for YCo_5 . *Phys. Rev. B* **2014**, *90*, 054421-1–054421-11. [[CrossRef](#)]
72. Tozman, P.; Vinkatesan, M.; Zickle, G.A.; Fidler, J.; Coey, J.M.D. Enhanced energy product in Y-Co-Fe magnets intermediate between Nd-Fe-B and ferrite. *Appl. Phys. Lett.* **2015**, *107*, 032405-1–032405-4. [[CrossRef](#)]
73. Tozman, P.; Vinkatesan, M.; Coey, J.M.D. Optimization of the magnetic properties of nanostructured Y-Co-Fe alloys for permanent magnets. *AIP Adv.* **2016**, *6*, 056016-1–056016-5. [[CrossRef](#)]
74. Patrick, C.E.; Kumar, S.; Balakrishnan, G.; Edwards, R.S.; Lees, M.R.; Mendive-Tapia, E.; Petit, L.; Staunton, J.B. Rare-earth/transition-metal magnetic interactions in pristine and (Ni,Fe)-doped YCo_5 and $GdCo_5$. *Phys. Rev. Mater.* **2017**, *1*, 024411-1–024411-13. [[CrossRef](#)]
75. Patrick, C.E.; Staunton, J.B. Rare-earth/transition-metal magnets at finite temperature: Self-interaction-corrected relativistic density functional theory in the disordered local moment picture. *Phys. Rev. B* **2018**, *97*, 224415-1–224415-15. [[CrossRef](#)]

76. Patrick, C.E.; Kumar, S.; Balakrishnan, G.; Edwards, R.S.; Lees, M.R.; Petit, L.; Staunton, J.B. Calculating the Magnetic Anisotropy of Rare-Earth–Transition-Metal Ferrimagnets. *Phys. Rev. Lett.* **2018**, *120*, 097202. [[CrossRef](#)] [[PubMed](#)]
77. Burzo, E.; Vlaic, P.; Kozlenko, D.P.; Golosova, N.O.; Kichanov, S.E.; Savenko, B.N.; Östlin, A.; Chioncel, L. Structure and magnetic properties of YCo₅ compound at high pressures. *JMST* **2020**, *42*, 106–112. [[CrossRef](#)]
78. Sakurai, M.; Wu, S.; Zhao, X.; Nguyen, M.C.; Wang, C.-Z.; Ho, K.-M.; Chelikowsky, J.R. Magnetocrystalline anisotropy in YCo₅ and ZrCo₅ compounds from first-principles real-space pseudopotentials calculations. *Phys. Rev. Mater.* **2018**, *2*, 084410-1–084410-5. [[CrossRef](#)]
79. Nguyen, M.C.; Yao, Y.; Wang, C.-Z.; Ho, K.-M.; Andropov, V.P. Magnetocrystalline anisotropy in cobalt based magnets: A choice of correlation parameters and the relativistic effects. *J. Phys. Condens. Matter* **2018**, *30*, 195801-1–195801-8. [[CrossRef](#)]
80. Soderžnik, M.; Korent, M.; Žagar Soderžnik, K.; Dubois, J.-M.; Tozman, P.; Venkatesan, M.; Coey, J.M.D.; Kobe, S. Hot-compaction of YCo_{4.8}Fe_{0.2} nanocrystals for metal-bonded magnets. *J. Magn. Magn. Mater.* **2018**, *460*, 401–408. [[CrossRef](#)]
81. Patrick, C.E.; Matsumoto, M.; Staunton, J.B. First-principles calculations of the magnetocrystalline anisotropy of the prototype 2:17 cell boundary phase. *J. Magn. Magn. Mater.* **2019**, *477*, 147–155. [[CrossRef](#)]
82. Patrick, C.E.; Staunton, J.B. Temperature-dependent magnetocrystalline anisotropy of rare earth/transition metal permanent magnets from first principles: The light RCo₅ (R=Y, La-Gd) intermetallics. *Phys. Rev. Mater.* **2019**, *3*, 101401-1–101401-7. [[CrossRef](#)]
83. Asali, A.; Fidler, J.; Suess, D. Influence of changes in electronic structure on magnetocrystalline anisotropy of YCo₅ and related compounds. *J. Magn. Magn. Mater.* **2019**, *485*, 61–68. [[CrossRef](#)]
84. Ucar, H.; Choudhary, R.; Paudyal, D. Substitutional and interstitial doping in LaCo₅ system for the development of hard magnetic properties: A first principles study. *J. Magn. Magn. Mater.* **2020**, *496*, 165902-1–165902-8. [[CrossRef](#)]
85. Subramanian, P.R.; Smith, J.F. Thermodynamics of formation of Y-Co alloys. *Metall. Trans. A* **1985**, *16*, 1195–1201. [[CrossRef](#)]
86. Wu, C.H.; Chuang, Y.C. The Co-Y (Cobalt-Yttrium) system. *J. Phase Equilibria Diffus.* **1991**, *12*, 587–592. [[CrossRef](#)]
87. Shevchenko, M.A.; Ivanov, M.I.; Berezutski, V.V.; Kudin, V.G.; Sudavtsova, V.S. Thermodynamic properties of alloys of the Co-Sc and Co-Y systems. *Russ. J. Phys. Chem. A* **2015**, *89*, 931–940. [[CrossRef](#)]
88. Du, Z.; Zhang, W.; Zhao, L. Thermodynamic Assessment of Co-Y System. *Rare Metals* **1996**, *15*, 185–190.
89. Du, Z.; Lü, D. Thermodynamic modelling of the Co–Y system. *J. Alloy. Compd.* **2004**, *373*, 171–178. [[CrossRef](#)]
90. Golumbskie, W.; Liu, Z.-K. CALPHAD/first-principles re-modeling of the Co–Y binary system. *J. Alloy. Compd.* **2006**, *407*, 193–200. [[CrossRef](#)]
91. Gupta, K.G. The Co-Ni-Y (Cobalt-Nickel-Yttrium) system. *J. Phase Equilibria Diffus.* **2010**, *31*, 389–394. [[CrossRef](#)]
92. Du, Z.; Lü, D. Thermodynamic modeling of the Co–Ni–Y system. *Intermetallics* **2005**, *13*, 586–595. [[CrossRef](#)]
93. Golumbskie, W.J.; Prins, S.N.; Eden, T.J.; Liu, Z.-K. Predictions of the Al-rich region of the Al–Co–Ni–Y system based upon first-principles and experimental data. *Calphad* **2009**, *33*, 124–135. [[CrossRef](#)]
94. Chuang, Y.C.; Wu, C.H.; Chang, Y.C. Study of the 1050 °C isothermal section of the ternary system Y-Co-Fe. *J. Less-Common Met.* **1986**, *118*, 7–20. [[CrossRef](#)]
95. Kharchenko, O.I.; Bodak, O.I.; Gladyshevskii, E.I. Interaction of Yttrium with metals of the iron family. *Russ. Metall.* **1977**, *1*, 170–176.
96. Söderlind, P.; Turchi, P.E.A.; Landa, A.; Lordi, V. Ground-state properties of rare-earth metals: An evaluation of density-functional theory. *J. Phys. Condens. Matter* **2014**, *26*, 416001-1–416001-8. [[CrossRef](#)]
97. Landa, A.; Söderlind, P.; Parker, D.; Åberg, D.; Lordi, V.; Perron, A.; Turchi, P.E.A.; Chouhan, R.K.; Paudyal, D.; Lograsso, T.A. Thermodynamics of the SmCo₅ compound doped with Fe and Ni: An ab initio study. *J. Alloys Compd.* **2018**, *765*, 659–663. [[CrossRef](#)]
98. Vitos, L. Total-energy method based on the exact muffin-tin orbital theory. *Phys. Rev. B* **2001**, *64*, 014107-1–014107-11. [[CrossRef](#)]
99. Vitos, L. *Computational Quantum Mechanics for Materials Engineers: The EMTO Method and Application*; Springer: London, UK, 2007.

100. Kollar, J.; Vitos, L.; Skriver, H.L. From ASA towards the Full Potential. In *Lecture Notes in Physics*; Dreyssé, H., Ed.; Springer: Berlin, Germany, 2000; pp. 85–113.
101. Perdew, J.P.; Burke, K.; Ernzerhof, M. Generalized gradient approximation made simple. *Phys. Rev. Lett.* **1996**, *77*, 3865–3868. [[CrossRef](#)]
102. Chadi, D.J.; Cohen, M.L. Special Points in the Brillouin Zone. *Phys. Rev. B* **1973**, *8*, 5747–5753. [[CrossRef](#)]
103. Pourovskii, L.V.; Ruban, A.V.; Vitos, L.; Ebert, H.; Johansson, B.; Abrikosov, I.A. Fully relativistic spin-polarized exact muffin-tin-orbital method. *Phys. Rev. B* **2005**, *71*. [[CrossRef](#)]
104. Faulkner, J.S. The modern theory of alloys. *Prog. Mater. Sci.* **1982**, *27*, 1–187. [[CrossRef](#)]
105. Vitos, L.; Abrikosov, I.A.; Johansson, B. Anisotropic lattice distortions in random alloys from first-principles theory. *Phys. Rev. Lett.* **2001**, *87*. [[CrossRef](#)] [[PubMed](#)]
106. Ruban, A.V.; Skriver, H.L. Screened Coulomb interaction in metallic alloys. I. Univesal screening in the atomic sphere approximations. *Phys. Rev. B* **2002**, *66*, 66. [[CrossRef](#)]
107. Ruban, A.V.; Simak, S.I.; Korzhavyi, P.A.; Skriver, H.L. Screened Coulomb interaction in metallic alloys. II. Screening beyond the single-site and atomic-sphere approximations. *Phys. Rev. B* **2002**, *66*, 024202-1–024202-12. [[CrossRef](#)]
108. Ruban, A.V.; Simak, S.I.; Shallcross, S.; Skriver, H.L. Local Lattice relaxations in random metallic alloys: Effective tetrahedron model and supercell approach. *Phys. Rev. B* **2003**, *67*, 214302-1–214302-12. [[CrossRef](#)]
109. Staunton, J.; Gyorffy, B.; Pindor, A.; Stocks, G.M.; Winter, H. The “disordered local moment” picture of itinerant magnetism at finite temperatures. *J. Magn. Magn. Mater.* **1984**, *45*, 15–22. [[CrossRef](#)]
110. Gyorffy, B.L.; Pindor, A.; Staunton, J.; Stocks, G.M.; Winter, H. A first-principles theory of ferromagnetic phase transitions in metals. *J. Phys. F Met. Phys.* **1985**, *15*, 1337–1386. [[CrossRef](#)]
111. Murnaghan, F.D. The compressibility of media under extreme pressures. *Proc. Natl. Acad. Sci. USA* **1944**, *30*, 244–247. [[CrossRef](#)]
112. Andersen, O.K. Linear methods in band theory. *Phys. Rev. B* **1975**, *12*, 3060–3083. [[CrossRef](#)]
113. Söderlind, P. Delocalization and phase transitions in Pr: Theory. *Phys. Rev. B* **2002**, *65*, 115105-1–115105-5. [[CrossRef](#)]
114. Wills, J.M.; Alouani, M.; Andersson, P.; Delin, A.; Eriksson, O.; Grechnev, O. *Full-Potential Electronic Structure Method*; Springer Series in Solid-State Science; Springer: Berlin/Heidelberg, Germany, 2010; Volume 167.
115. von Barth, U.; Hedin, L. A local exchange-correlation potential for the spin polarized case. i. *J. Phys. C* **1972**, *5*, 1629–1642. [[CrossRef](#)]
116. Kaufman, L.; Bernstein, H. *Computer Calculation of Phase Diagrams with Special Reference to Refractory Metals*; Academic Press: New York, NY, USA, 1970.
117. Saunders, N.; Miodownik, A. *CALPHAD Calculation of Phase Diagrams: A Comprehensive Guide*; Elsevier Science: New York, NY, USA, 1998.
118. Lukas, H.; Fries, S.; Sundman, B. *Computational Thermodynamics: The CALPHAD Method*; Cambridge University Press: Cambridge, UK, 2007.
119. Sundman, B.; Jansson, B.; Andersson, J.-O. The Thermo-Calc databank system. *Calphad* **1985**, *9*, 153–190. [[CrossRef](#)]
120. Andersson, J.-O.; Helander, T.; Höglund, L.; Shi, P.; Sundman, B. Thermo-Calc & DICTRA, computational tools for materials science. *Calphad* **2002**, *26*, 273–312. [[CrossRef](#)]
121. Du, Z.; Zhang, W.; Zhuang, Y. Thermodynamic Assessment of the Fe-Y System. *Rare Metals* **1997**, *16*, 52–58.
122. Lü, D.; Guo, C.; Li, C.; Du, Z. Thermodynamic description of Fe–Y and Fe–Ni–Y systems. *Phys. Procedia* **2013**, *50*, 383–387. [[CrossRef](#)]
123. Konar, B.; Kim, J.; Jung, I.-H. Critical systematic evaluation, and thermodynamic optimization of the Fe-RE system: RE = Gd, Tb, Dy, Ho, Er, Tm, Lu, and Y. *J. Phase Equilibria Diffus.* **2017**, *38*, 509–542. [[CrossRef](#)]
124. Kardellass, S.; Servant, C.; Selhaoui, N.; Iddaoudi, A.; Ait Amar, M.; Bouirden, L. Thermodynamic assessments of the Fe-Y and Ni-Sc systems. *MATEC Web Conf.* **2013**, *3*, 01008-1–01008-6. [[CrossRef](#)]
125. Kardellass, S.; Servant, C.; Selhaoui, N.; Iddaoudi, A.; Ait Amar, M.; Bouirden, L. A thermodynamic assessment of the iron–yttrium system. *J. Alloy. Compd.* **2014**, *583*, 598–606. [[CrossRef](#)]
126. Saenko, I.; Fabrichnaya, O.; Udovsky, A. new thermodynamic assessment of the Fe-Y system. *J. Phase Equilibria Diffus.* **2017**, *38*, 684–699. [[CrossRef](#)]
127. Du, Z.; Zhang, W. Thermodynamic assessment of the Ni-Y system. *J. Alloy. Compd.* **1996**, *245*, 164–167. [[CrossRef](#)]

128. Mattern, N.; Zinkevich, M.; Löser, W.; Behr, G.; Acker, J. Experimental and Thermodynamic Assessment of the Nb-Ni-Y System. *J. Phase Equilibria Diffus.* **2008**, *29*, 141–155. [[CrossRef](#)]
129. Huang, J.; Yang, B.; Chen, H.; Wang, H. Thermodynamic optimization of the Ni-Al-Y ternary system. *J. Phase Equilibria Diffus.* **2015**, *36*, 357–365. [[CrossRef](#)]
130. Mezbahul-Islam, M.; Medraj, M. A critical thermodynamic assessment of the Mg–Ni, Ni–Y binary and Mg–Ni–Y ternary systems. *Calphad* **2009**, *33*, 478–486. [[CrossRef](#)]
131. Subramanian, P.R.; Smith, J.F. Thermodynamics of formation of Y-Ni alloys. *Metall. Trans. B* **1985**, *16*, 577–584. [[CrossRef](#)]
132. Okamoto, H. Supplemental Literature Review of Binary Phase Diagrams: Cd-Se, Cu-Hg, Cu-Ho, Eu-Mg, H-Sr, Hf-Si, La-Mn, Mn-Nd, Nb-Y, Ni-Y, Pb-Se, and Sc-Sr. *J. Phase Equilibria Diffus.* **2013**, *34*, 430–436. [[CrossRef](#)]
133. Sato, K.; Katayama-Yoshida, H.; Dederichs, P. Dilute magnetic semiconductors. *Newsletter* **2005**, *70*, 93–110.
134. Ma, D.; Grabowski, B.; Körmann, F.; Neugebauer, J.; Raabe, D. Ab initio thermodynamics of the CoCrFeMnNi high entropy alloy: Importance of entropy contributions beyond the configurational one. *Acta Mater.* **2015**, *100*, 90–97. [[CrossRef](#)]
135. Coey, M.D. *Magnetism and Magnetic Materials*; Cambridge University Press: Cambridge, UK, 2010; p. 471.
136. Ekholm, M.; Gambino, D.; Jönsson, H.J.M.; Tasnádi, F.; Alling, B.; Abrikosov, I.A. Assessing the SCAN functional for itinerant electron ferromagnets. *Phys. Rev. B* **2018**, *98*, 094413-1–094413-7. [[CrossRef](#)]



© 2020 by the authors. Licensee MDPI, Basel, Switzerland. This article is an open access article distributed under the terms and conditions of the Creative Commons Attribution (CC BY) license (<http://creativecommons.org/licenses/by/4.0/>).